Medical University of Vienna
Center of Biomedical Research
(Head: Univ.-Prof. Dr. Bruno Podesser)

Analysis of molecular mechanisms involved in calcification of porcine cardiac valve cells

Bachelor thesis

University of Veterinary Medicine Vienna

Submitted by
Nele Aigner

Vienna, July 2021

Internal supervisor: Ao. Univ.-Prof. Dr. med. vet. Rupert Palme

External supervisor: Mag. Dr. Barbara Kapeller

Reviewer: Ao. Univ.-Prof. Mag. rer. nat. Dr. rer. nat. Ingrid Walter

Acknowledgements

I would like to express my very deep gratitude to the whole team of the Department of Biomedical Research for their assistance at every stage of this research project.

I would also like to thank Dr. Rupert Palme for his support and trust during my bachelor thesis.

1. Table of Contents

2. Introduction

The leading causes of death worldwide are related to cardiovascular diseases. In 2019, the highest cause of death, representing 16 % of all deaths worldwide, is ischemic heart disease; followed by stroke, which is the second leading cause of death (World Health Organization; https://www.who.int/news-room/fact-sheets/detail/the-top-10-causes-of-death (Access: 24.06.2021)).

2.1. Anatomy and functions of the cardiovascular system

The cardiovascular system is a perfectly coordinated, complex system that consists of the heart and blood vessels. Its main task is to supply the organism with oxygen, nutrients, and hormones, and to dispose of carbon dioxide and other used metabolites. For this purpose, a constant circulation of the blood must be ensured. The blood is transported through vessels, which are tubular hollow organs that consist of three main layers. As can be seen in **fig. 1**, the innermost layer (*Tunica intima*) consists of endothelial cells and ensures the exchange of nutrients and gases between the blood and the vessel wall. The middle layer (*Tunica media*) consists of smooth muscle cells and elastic connective tissue, and the outermost layer (*Tunica adventitia*) consists of collagen and elastic fibers (Pugsley and Tabrizchi 2000).

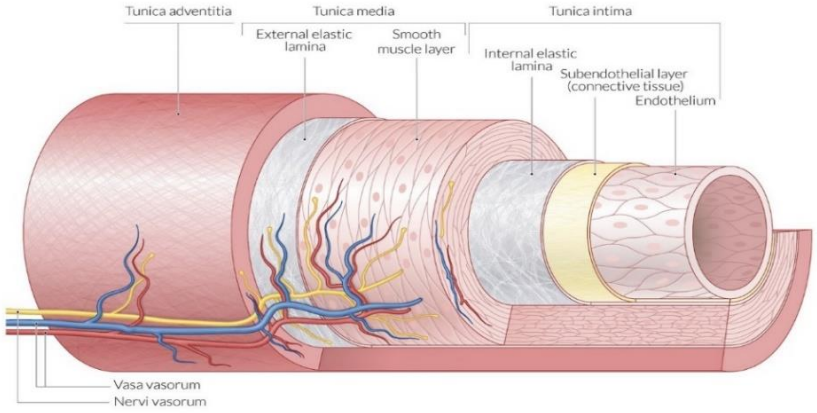

Figure 1 Schematic structure of a blood vessel (https://www.amboss.com/us/knowledge/Blood_vessels/, Access: 12.07.2021)

Through the vascular system, oxygenated, nutritious blood is transported to the organs, meanwhile deoxygenated blood flows into the lungs, where it is re-oxygenated. This newly oxygenated blood flows through the pulmonary veins to the left atrium and further through the mitral valve into the left ventricle. Blood leaves the heart via the aortic valve **(fig. 2)** through the aorta, which branches into arteries, arterioles, and capillary beds. In the capillaries, the delivery of oxygen and nutrients to the tissue and the absorption of carbon dioxide and used metabolites occurs. The deoxygenated blood is pumped through the veins, which merge as the vena cava superior and the vena cava inferior, and enters the heart through the right atrium. The blood flows into the right ventricle via the tricuspid valve and enters the pulmonary trunk through the pulmonary valve, to the lungs, where it is supplied with oxygen again.

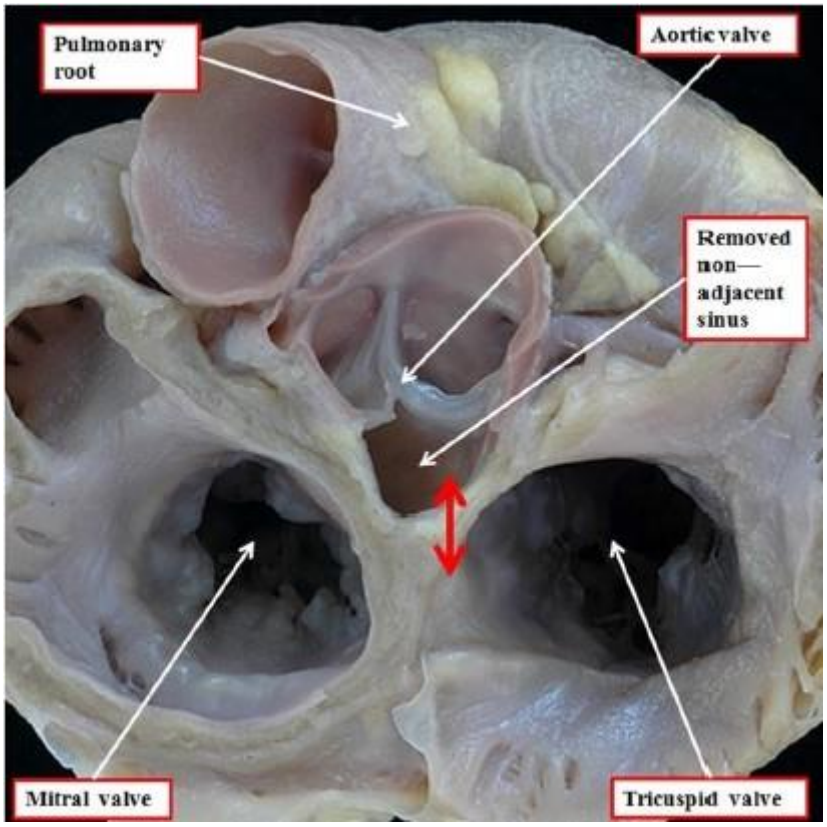

Figure 2 The short cardiac axis, photographed from the atrial aspect. The aortic valve is located centrally and overlaps with the mitral valve. The aortic valve leaflets have been removed (Spicer, et al. 2014).

The four different valves are essential in the cardiovascular system, as they are functioning as outlets and prevent the backflow of blood in the wrong direction. In this work, we are focusing on the aortic valve **(fig. 3)** that is attached to the fibrous ring at the outlet of the left ventricle and consists of three semilunar leaflets, which are formations of the *Tunica intima*. These leaflets are in constant motion, at the beginning of the diastole, they prevent the backflow of blood and during systole, they are pushed to the walls of the ascending aorta by the blood.

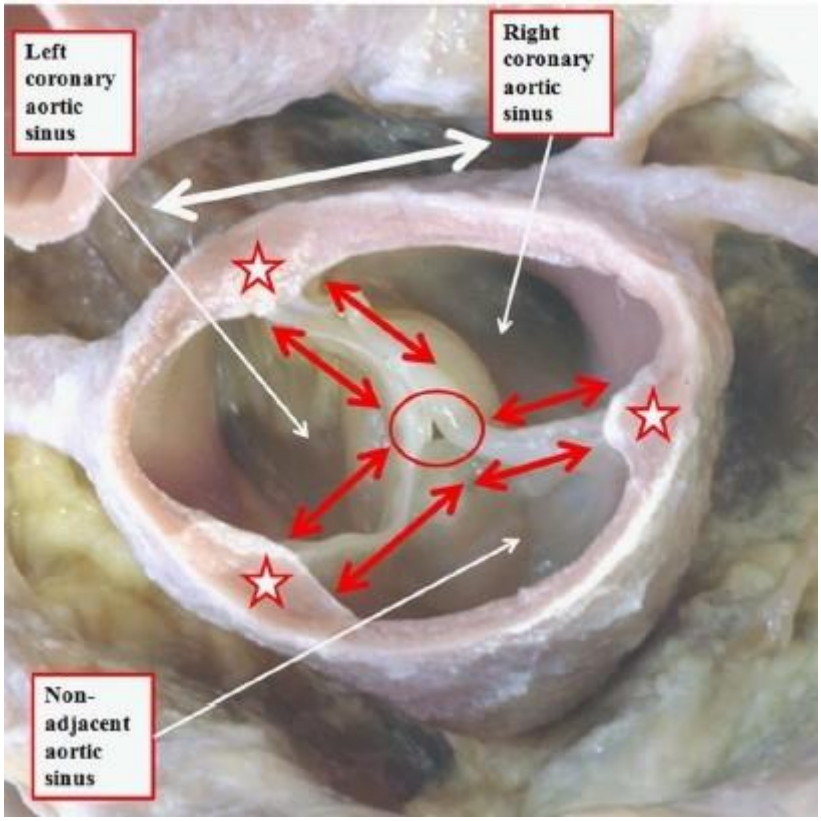

Figure 3 Closed aortic valve with the three semilunar leaflets, photographed from the arterial aspect (Spicer, et al. 2014).

2.2. Calcification of cardiac valves and blood vessels

Calcification is a major health problem, which becomes more frequent with aging. In aortic valve stenosis, the calcification affects the aortic valve leaflets; they get fibrous, larger in diameter, and stiffer which leads to an insufficient opening and closing **(fig. 4).** Since the valves can no longer perform their physiological function properly, the heart has to increase its pumping rate to compensate for the valvular dysfunction. Considering there is currently no effective drug treatment, aortic valve stenosis must usually be treated surgically. This involves removing the damaged valve and replacing it with a biological or prosthetic valve, which is an especially risky procedure for patients of advanced age (Rutkovskiy, et al. 2017).

Another widespread disease related to calcification is atherosclerosis, which is the most common underlying cause of coronary artery disease. Here, the calcification affects the blood vessels, already starting in childhood as fatty streaks that later progress to raised lesions and further to mature atheroma that contain mineral deposition in the form of calcium-phosphate complexes. Due to mineral depositions, the arteries get stiffer and the vessel walls can weaken to such an extent that it dilates and an aneurysm develops (Allison, et al. 2004). Moreover, atheroma or atherosclerotic plaque **(fig. 5)** can impair and block the blood flow, which increases the probability that a thrombus forms at the plaque that can lead to infarction and death (Falk 2006).

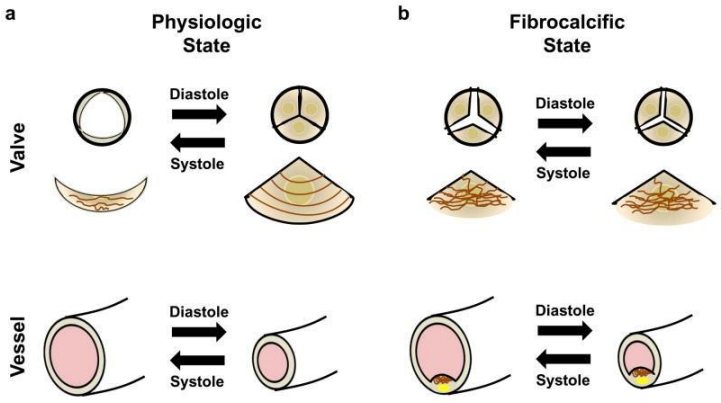

Figure 4 Schematic comparison of a a) physiological cardiac valve and a blood vessel to a b) calcified valve and vessel (Hutcheson, et al. 2014).

Figure 5 Left: Extensively calcified aortic valve; Middle and right: Hematoxylin/eosin stain of atherosclerotic plaque. The black mark indicates calcification (CA), arrow indicates cholesterol crystals (Johnson, et al. 2006).

Vascular and valvular calcification is a multifaceted process that is far from being completely understood. It is well established that calcification is an active process in which changes in signaling pathways can lead to the deposition of hydroxyapatite. These signaling pathways are highly complex interlinked and are influenced by intracellular and extracellular factors (Yuan, et al. 2021).

2.3. Signaling pathways

2.3.1. Hippo Signaling

The most important functions of the Hippo pathway are cell proliferation and differentiation in developing organs. In healthy adults, the Hippo pathway limits tissue growth. Thus, as dysregulation of the Hippo pathway can lead to abnormal cell growth, the Hippo pathway can function as a tumor suppressor.

The Hippo pathway reacts to many different stimuli, including mechanical cues, cell-cell contact, inflammation, epithelial-to-mesenchymal transition, and osmotic stress.

The core of the mammalian Hippo pathway is a kinase cascade **(fig. 6)**, wherein the active mammalian Ste20-like kinase1/2 (MST1/2) and Salvador family WW domain-containing protein 1 (SAV1) form a complex. This complex, together with the scaffold protein MOB kinase activator 1A/B (MOB1A/B) phosphorylates, activates Large tumor suppressor (LATS1/2). This core kinase cascade inhibits Yes-associated protein (YAP) and Transcriptional coactivator with PDZ-binding motif (TAZ) through phosphorylation. When YAP/TAZ is phosphorylated, it binds to 14-3-3 that is involved in tight and adherence junctions, and remains in the cytoplasm and further leads to beta-transducin repeat containing E3 ubiquitin protein ligase (β-TrCP)-mediated YAP/TAZ polyubiquitination and proteasomal degradation. When dephosphorylated, YAP/TAZ translocates into the nucleus. As YAP and TAZ do not have DNA-binding domains, they bind to TEA domain transcription factors 1—4 (TEAD1—4). Through this interaction, YAP/TAZ can up and down-regulate the expression of a wide range of genes that are involved in cell proliferation and tumorgenesis (Meng, et al. 2016).

Moreover, the Hippo pathway intercommunicates with other pathways, like the Wingless/Ints (Wnt) pathway **(fig.9)**. Signals of this pathways can also modulate the activity of YAP and TAZ.

1.1.1. Wingless/Ints (Wnt)/β-Catenin Signaling

The Wnt/β-Catenin pathway is very important in embryonic development, especially in the development of the heart, subsequently, issues or mutations in this pathway can lead to cancer. Wnt-family proteins are growth-stimulating factors that are incorporated in exosomes for transport through the body. β-Catenin is a scaffold protein that can influence transcription and is regulated by degradation.

If a Wnt ligand binds to a family of seven transmembrane receptors named Frizzled, Frizzled phosphorylates Lipoprotein-related-receptor protein (LRP5/6) and forms a large complex with it. When LRP5/6 is phosphorylated, it binds to Disheveled (DVL), which is part of the destruction complex. This complex involves DVL, AXIN, glycogen synthase kinase 3 (GSK3), β-catenin, casein kinase 1 (CK1), adenomatous polyposis coli (APC), and β-TrCP, which is an ubiquitin ligase. β-catenin is then translocated to the nucleus where it binds to T-cell factor/lymphoid enhancer factor (LEF/TCF) transcription factors **(fig. 7)**.

In the absence of Wnt signals, β-catenin is ubiquitinated by the destruction complex and degradated through β-TrCP. Consequently, β-catenin cannot translocate to the nucleus to regulate gene expression (Piersma, et al. 2015).

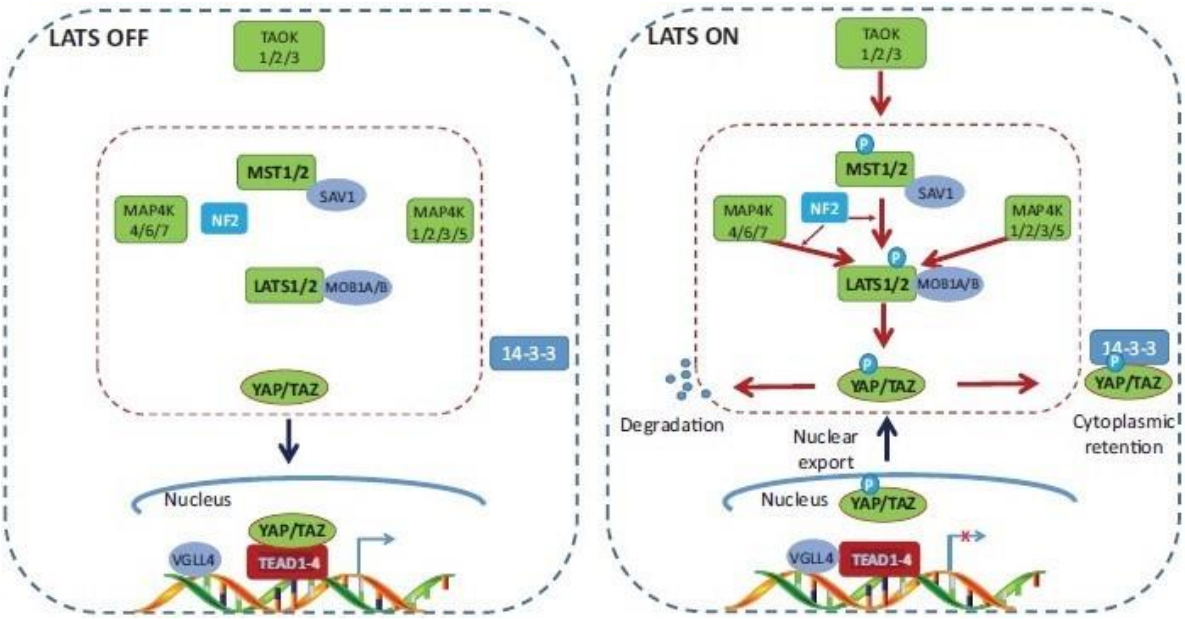

Figure 6 The mammalian Hippo pathway (Meng, et al. 2016).

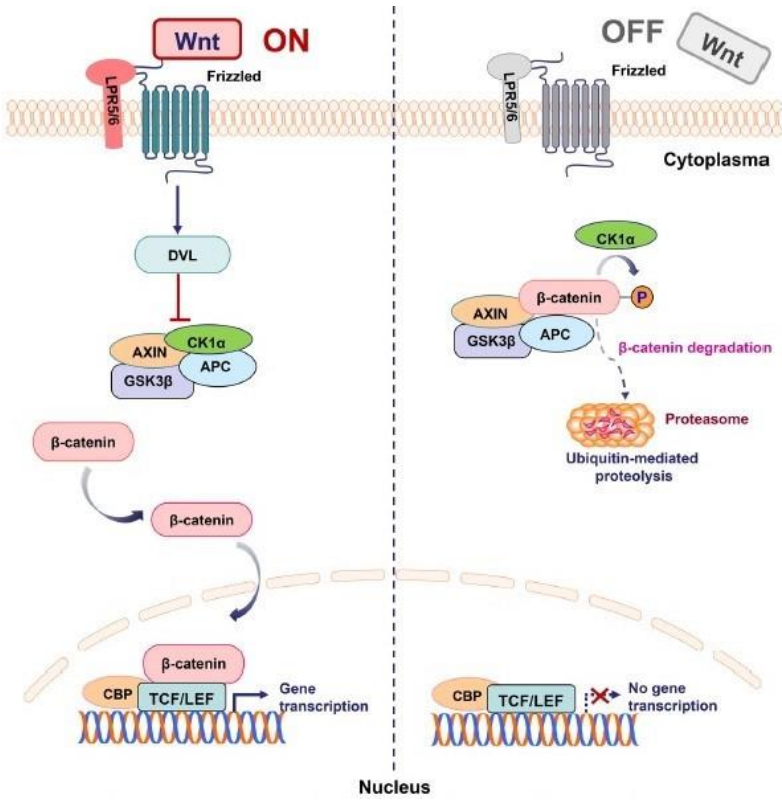

Figure 7 Wnt/ β-Catenin signaling (Zhang and Wang 2020).

2.3.2. Transforming growth factor-β (TGF-β) Signaling

The TGF-β signaling pathway **(fig. 8)** plays an essential role in cell growth, development, and differentiation. Signaling is initiated by the binding of TGF-β or bone morphogenetic protein (BMP) ligands to a type l or ll receptor. Under physiological conditions, TGF-β is retained in the extracellular matrix (ECM), but injury, integrin binding, or mechanical stress releases TGF-β from the ECM and allows it to interact with its receptors.

TGF-β binds to a heterotetrameric complex of two type l and two type ll receptors. The cascade can be inhibited by an inhibitory (I-) SMAD protein, SMAD7, and Smad-specific E3 ubiquitin-protein ligases (Smurf) by targeting it for ubiquitination. The activated receptor complex can bind and phosphorylate regulatory (R-) SMAD proteins. SMAD2/3 are activated by the TGF-β/activing pathway and SMAD1/5/9 by the BMP pathway. Both, regulatory SMAD2/3 and SMAD1/5/9 bind to co-activator (Co-) SMAD, SMAD4, and translocate into the nucleus where they form a complex with several transcription factors and co-factors to initiate the transcription of specific genes (Hu, et al. 2018).

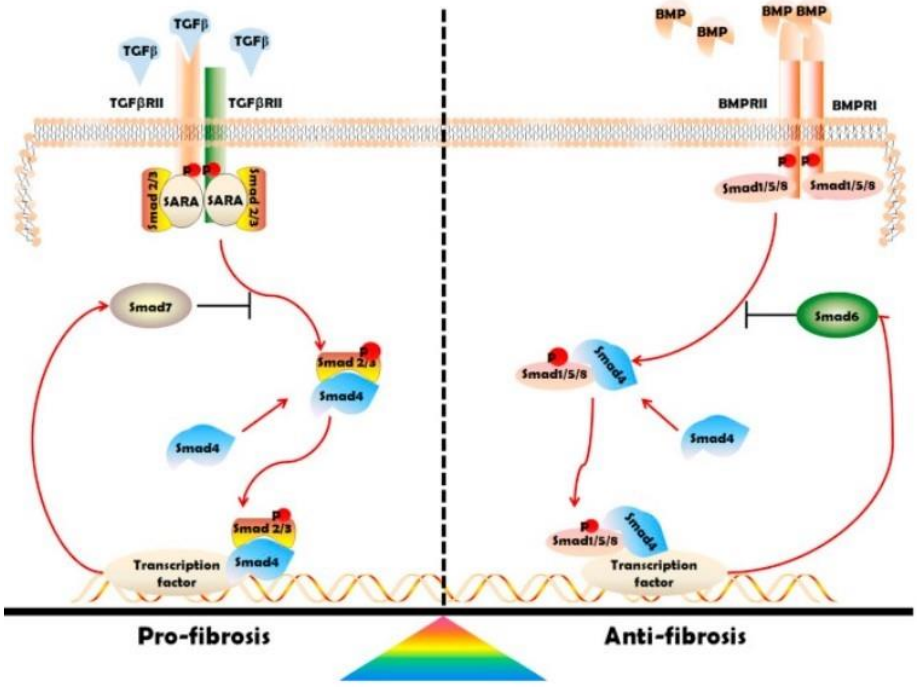

Figure 8 TGF-β signaling (Hu, et al. 2018).

2.3.3. Crosstalk between Hippo, Wnt, and TGF- β signaling

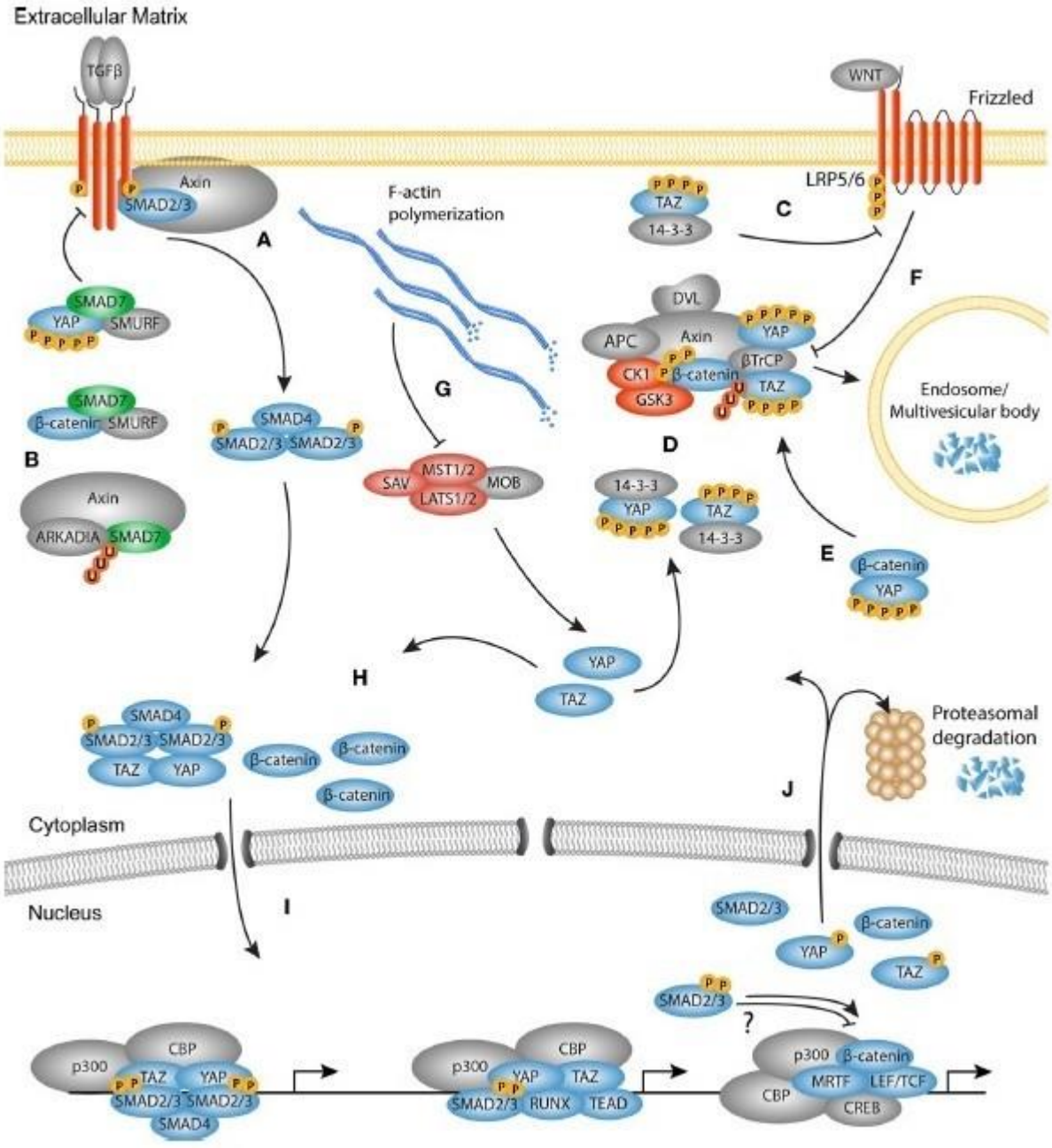

Figure 9 Mechanistic overview of the cross talk between YAP/TAZ, Wnt, and TGF-β signaling (Piersma, et al. 2015).

A-B: When TGF-β binds to its receptor, AXIN supports the activation of SMAD2/3. Moreover, AXIN additionally increases TGF-β signaling by promoting degradation of the inhibitory Smad protein, SMAD7. SMAD7 can bind to both YAP and β-catenin. The YAP/SMAD7 complex increases affinity for the type I receptor and thus enhances the inhibitory effects of SMAD7.

C: TAZ can inhibit the activation of disheveled (DVL) and therefore regulates Wnt-signaling.

D + F + G: Phosphorylated YAP and TAZ can either bind to 14-3-3 proteins or attach to the β-catenin destruction complex where YAP/TAZ is essential for the docking of β-TrCP. Wnt3a stimulation induces YAP/TAZ to disengage itself from the destruction complex, which leads to high levels of β-catenin, as β-TrCP cannot bind and ubiquitinate β-catenin. Furthermore, leads the polymerization of the F-actin cytoskeleton to high levels of β-catenin that can accumulate in the cytoplasm, as the polymerized F-actin inhibits the activity of MST1/2.

E: Phosphorylated YAP binds to and activates β-catenin. Consequently, β-catenin cannot translocate into the nucleus and is degradated. Thus, increased Hippo signaling not only leads to higher levels of phosphorylated YAP but consequently also to lower levels of nuclear β-catenin.

H: YAP/TAZ can interact with the activated SMAD2/3-SMAD4-complex and thereby promoting the nuclear accumulation of SMAD2/3. This leads to increased transcriptional activity on SMAD2/3 target genes. The expression and activation of YAP/TAZ seem to control SMAD accumulation.

I: Nuclear transcription factors can co-localize to enhance or inhibit the transcriptional activity and thence regulate the transcription of epithelial-to-mesenchymal transition (EMT) related genes (Piersma, et al. 2015).

2.4. Endothelial-mesenchymal transition (EndoMT)

Endothelial-mesenchymal transition is induced by specific stimuli **(fig. 10)**, including transforming TGF-β, Wnt/β-catenin, and Hippo signaling pathway, hypoxia, inflammation, or oxidative stress. During this transition, endothelial cells lose their characteristic features, such as platelet endothelial cell adhesion molecule-1 (CD31) and Von Willebrand factor (VWF), and transform into cells with mesenchymal characteristics, that have high levels of α-smooth muscle actin (α-SMA) and vimentin, and these mesenchymal cells can further transform into osteoblast-like cells. EndoMT is a physiological process during normal embryogenesis or woundhealing. Prolonged or extensive EndoMT, however, can lead to atherosclerosis, valvular heart disease, and vascular calcification (Quaglino, et al. 2020).

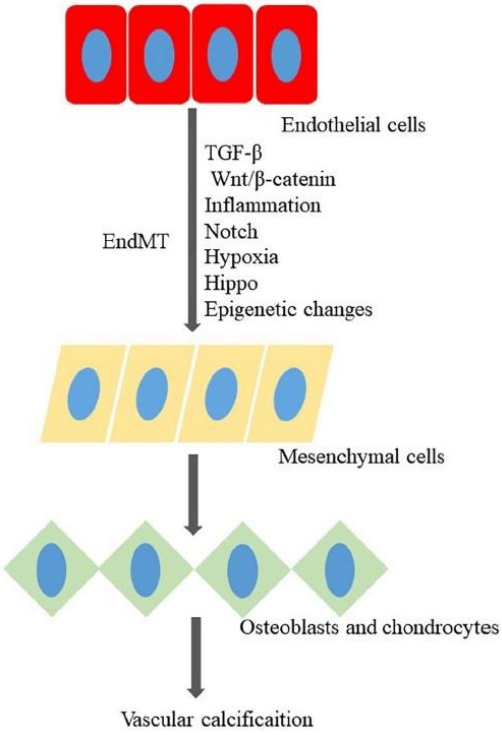

Figure 10 Schematic representation of the calcification process (Yuan, et al. 2021)

2.5. Mechanical signals

Mechanical signals are generated from cell-cell contacts; cell-extracellular matrix (ECM) interaction and the microenvironment have been recognized to regulated gene transcription and coordinate during proliferation morphogenesis and migration (Ma, et al. 2019). In general, by high stiffness or stretching some signaling pathways are involved and promote the expression of proteins important in calcified cells.

In bone, mechanical stress is an important promoter and regulator of formation and development; in soft tissue, though, it can lead to pathological processes, known as ectopic calcification. Through increased mechanical stress, many proteins, originally associated with bone tissue, are also expressed in calcified vascular tissue (Tyson, et al. 2020).

2.6. Osteoprotegerin (OPG) and Osteopontin (OPN)

It is already established that Osteoprotegerin and Osteopontin play an important role in calcification in atherosclerosis and the calcification of cardiac valves (Kawakami, et al. 2016). However, the exact mechanisms and correlations have not been completely elucidated yet and probably dependent on context and type of cell.

In vivo, OPG is expressed by osteoblasts, endothelial cells, smooth muscle cells and bone marrow stroma cells (Venuraju, et al. 2010) and involved in the Receptor activator of nuclear factor kappa-B ligand (RANKL)- Receptor activator of nuclear factor κ B (RANK)-OPG signaling pathway.

RANK is located on osteoclast precursors and mature osteoclasts and serves as a receptor for RANKL. RANKL, in contrast, is expressed by osteoblasts and plays a central role in osteoclast formation, function and survival. In bone, OPG inhibits the interaction between RANKL and RANK, and therefore is protective against bone loss (Boyce and Xing 2008).

Osteopontin (OPN) is an extracellular structural protein and is produced in many different cells, but mainly in bones. The regulation of the osteopontin gene is still not entirely understood either. However, it has already been discovered that there is a connection between the expression of OPN, inorganic phosphate and inflammatory processes (Fatherazi, et al. 2009; Icer and Gezmen-Karadag 2018).

2.7. Experimental structure of this work

As the mechanical strain is highly increased in calcified blood vessels and cardiac valves, a FlexCell FX-5000T™ Tension device was used, which allows the *in vitro* simulation of *in vivo* tissue strain. The device operates with a vacuum pressure that can induce different waveforms on cells. To mimic the pulsatile forces, normally induced by the heartbeat, we subjected cells to a cyclic stretch **(fig. 11 + 12).**

Since our aim in this work was to mimic the conditions of aortic valve stenosis and atherosclerosis, we not only subjected the cells to increased mechanical stress, but also added two different phosphate buffers to induce the process of calcification. One calcification media induces high levels of calcification, and the other does not only induce calcification, but also an inflammatory reaction.

To be able to analyze changes caused by calcification and mechanical stress at a molecular level, qPCRs and Western Blots were performed.

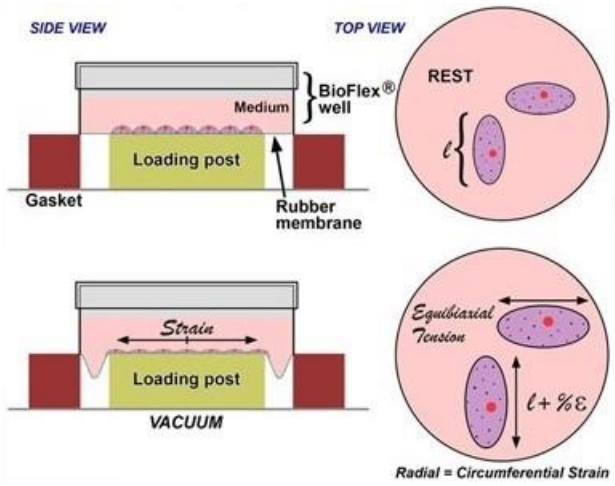

Figure 11 Schematic representation of mechanical strain induced by FlexCell FX-5000T™ (https://www.flexcellint.com/category/tension (Access: 18.06.2021))

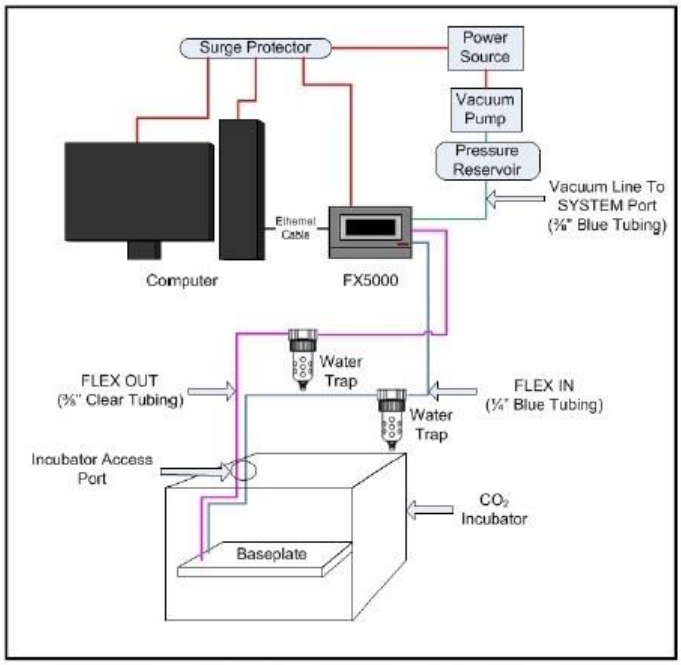

Figure 12 Set up of the FlexCell FX-5000T™ Tension System
(FlexCell FX-5000T™ Tension System user manual: https://www.google.com/url?sa=t&rct=j&q=&esrc=s&source=web&cd=&ved=2ahUKEwjpj4Ohi6HxAhUS16QKHbbgCEAQFjAKegQIBBAF&url=https%3A%2F%2Fuploads-ssl.webflow.com%2F5b916a469721fd4a8ae38199%2F5bb51acacac010cfa3ad914f_FX-5000TensionUsersManual.pdf&usg=AOvVaw0n9WiX109Dfj4LQVn-OD5w, (Access: 18.06.2021))

2.8. Aim of this study

The aim of this thesis was to observe the expression of genes that are related to calcification and mechanical stress, to create a better understanding of the molecular mechanisms involved in the development of calcification for further therapeutic approaches, or even prevention.

3. Material and methods

3.1. Cell culture

3.1.1. Cultivation media

Valvular endothelial cells (VEC), previously isolated from porcine aortic valves by collagenase II, were cultivated in Dulbecco's Modified Eagle Medium, high glucose, pyruvate (DMEM, Gibco, USA), supplemented with 10 % fetal bovine serum (FBS, Gibco, USA), 1 % Penicillin-Streptomycin (Pen/Strep, Gibco, USA) and 0.15 % Heparin (Sigma, USA). Vascular endothelial cells (EC), previously isolated from porcine aortas by collagenase II, were cultivated in DMEM, supplemented with 10 % Fetal Bovine Serum (FBS), 1 % Pen/Strep, 0.2 % Heparin, 0.2 % Endothelial Cell Growth Supplement (ECGS, BD Becton, Dickinson and Company, USA). The culture flasks were coated with laminin (20 µg/ml, Sigma, USA) before use and incubated for at least 15 minutes at 37 °C and 5 % CO_2. 1.25 ml laminin was used for 80 cm^2 flasks.

3.1.2. Cultivation and passaging of cells

The different cell isolations were grown in cultivation media in sterile culture flasks (Nunc, USA) in an incubator (HeraCell 150, Thermo Fischer, Austria) containing 5 % CO_2 at +37 °C and a relative humidity of 95 %. Care was taken to minimize movement of the culture plates at the beginning of cultivation to ensure adherence of the cells to the plate bottom. The medium was changed twice a week. In order to avoid too high cell densities and not to impair optimized growth conditions, the cells were always passaged in a subconfluent state. The culture medium was aspirated with a Pasteur pipette and the cells adhering to the bottom were carefully washed once with phosphate-buffered saline (PBS; Gibco, USA). To detach the cells from the culture flask, trypsin/ethylene diamine tetraacetic acid (EDTA) solution (Gibco, USA) was added once for 5 minutes, well distributed by gently shaking, and the cell layer was incubated for a few minutes at room temperature (RT). The cells detaching from the culture surface were collected in a centrifuge tube and centrifuged at 1200 rpm for 8 minutes at RT. The supernatant was aspirated and the pelleted cells were suspended in fresh culture medium at a ratio of 1:3 in new culture flasks.

3.1.3. Thawing of cells

Cells stored in liquid nitrogen were placed in a water bath at +37 °C and rapidly thawed. Then, cells were washed to remove dimethyl sulfoxide (DMSO) by slowly adding 10 ml of DMEM with additives and centrifugation for 8 min at 1200 rpm at RT. The cell pellet was then resuspended in fresh culture medium and transferred to a culture flask. To remove the DMSO completely, the medium was changed the next day.

3.1.4. Calcification media (CM)

To induce calcification, two different phosphate solutions, one with inorganic and one with organic phosphate, were prepared.

- The inorganic calcification media (CM1) consisted of 50 mM monosodium phosphate solved in PBS in the cultivation media.
- The organic calcification media (CM2) consisted of 445 mM ß-glycerophosphate, 7 mM ascorbic acid, and 7.5 nM dexamethasone in the cultivation media.

3.1.5. Cell counting

For cell counting, 50 µl of detached cell suspension was stained with 50 µl of 0.4 % trypan blue solution (Sigma, USA). This was followed by counting by hemocytometer. The non-viable cells stained blue, and the viable cells remained colorless. After counting all cells, the total cell count was determined and documented.

The total cell count was calculated using the following formula:

Total cell count = mean x dilution factor x 10^4 x initial volume in ml.

The viability of the cell culture was determined according to the following formula:

Viability = % live cells = unstained cells/total cell count x 100.

3.1.6. Cell freezing

At the time of freezing, cells were in the logarithmic growth phase. The cell layer was detached from the bottom of the flask by 1x trypsin/EDTA solution as described for passaging, and the cell material was collected by centrifugation for 8 minutes at 1200 rpm at RT. The supernatant was aspirated and the cells were resuspended with cold culture medium (+4 °C) plus 10 % DMSO and transferred into screw-capped cryotubes (Nunc, USA). These tubes were cooled at -80 °C for at least 24 hours and after the tubes were stored in liquid nitrogen at -196 °C.

3.1.7. Cell morphology

The morphology of the cells was examined and documented by light microscopy.

3.1.8. Fixation of cells

For cell characterization, cells were cultured on sterile glass slides in culture plates (Corning, USA). In the logarithmic growth phase, the culture medium was aspirated and the cells were washed with PBS. The slides were carefully removed from the culture dishes and the cells were fixed in cold 100 % acetone at +4 °C for 10 minutes. The slides were stored at -20 °C for the appropriate staining procedures.

3.2. Staining of cells

3.2.1. Immunofluorescence Staining

The previously fixed cells were washed in PBS and treated with 1 % H_2O_2 (Gatt Koller, Austria) to inhibit endogenous peroxidase activity. To avoid non-specific binding, the cells were incubated in blocking solution (2 % goat serum, Vector, USA, 1 % bovine serum albumin (BSA, Sigma-Aldrich, USA), 0.1 % gelatin (Sigma-Aldrich, USA), 0.1 % Triton-X-100 (Sigma-Aldrich, USA), 0.05 % Tween 20 (Promega, USA), PBS) and then incubated overnight with a primary antibody at 4 °C. The primary antibodies used were Von Willebrand Factor (VWF, rabbit, polyclonal antibody, Dako, Austria), smooth muscle actin (SMA, clone 1A4,

mouse, monoclonal antibody, Dako, Austria) and Platelet endothelial cell adhesion molecule (CD31, clone LCI-4, mouse, monoclonal antibody, Bio-Rad Laboraroies, USA). The next day, appropriately secondary antibodies (goat-anti-mouse, Alexa Fluor 488 or goat-anti-rabbit, Alexa Fluor 568) were applied and nuclear staining with 4′,6-diamidino-2-phenylindole (DAPI, Sigma, USA) was performed. The glass platelets were embedded with Flourescent Mounting Medium (Dako, Austria), microscopically analyzed (BX60, Olympus, USA), photographed with Nuance2 camera (Akoya Company, Biosciences, USA), and processed with the corresponding software Nuance2.8.0.

3.2.2. Alizarin Red Staining

Alizarin Red staining was performed to determine the presence of hydroxyapatite depositions, induced by osteogenic differentiation. Before staining, porcine vascular and valvular cells were cultivated in 24-well cultivation plates (Corning Inc., USA) on sterile glass slides in adequate cultivation medium, supplemented with CM1 or CM2, for 5 weeks. The cells were washed thrice with PBS thrice fixated in 70 % ethanol for one hour at –21 °C. After washing three times with distilled water, the cells were incubated with Alizarin Red solution (40 mM, pH=4.2, solved in 0.1 M PBS, Morphisto, USA)) for 10 minutes on shaker. The cells were washed and incubated over night in PBS at 4 °C. The next day, the fixed Alizarin Red was extracted with 10 % acetic acid for 30 minutes with shaking. Each well of the 24-well plate was distributed on 4 wells of a 96-well plate and the intensity of Alizarin Red was measured with a photometer at a wavelength of 405 nanometers. Outliners were excluded manually, and data statistically analyzed and visualized with the software “GraphPad Prism 5”.

3.3. Cyclic stretch experiments with a FlexCell FX-5000™ device

To mimic the pulsatile forces induced by the heartbeat, we subjected cells to a cyclic stretch by a FlexCell FX-5000™ device.

VEC and EC were detached from culture flasks with 0.05 % trypsin/EDTA and cell number and viability were determined by using trypan blue solution. Afterward, $1*10^6$ cells per well were seeded on 6-well BioFlex Culture Plates, coated with Collagen II. Seeding was performed in 1 ml of cell suspension per well, with and without the addition of 4 % CM1 and 4 % CM2 in the culture medium. Next, the plates were put on BioFlex Cell Seeders that limit cells to the central area of the membrane of a BioFlex Culture Plate. The FlexCell FX-5000™ Software was used to create a regimen. The settings are listed in **tab. 1** and **tab. 2**.

Table 1: Seeding program (long)

Step	Shape	Min	Max	Freq	DC %	Cycles	Duration
1	Static	0.0	15.0	1.0	50.0	39600	11 h
2	Static	0.0	13.0	1.0	50.0	39600	11 h
3	Static	0.0	11.0	1.0	50.0	39600	11 h
4	Static	0.0	9.0	1.0	50.0	360	6 min
5	Static	0.0	7.0	1.0	50.0	360	6 min
6	Static	0.0	5.0	1.0	50.0	360	6 min
7	Static	0.0	3.0	1.0	50.0	360	6 min
8	Static	0.0	1.0	1.0	50.0	360	6 min

Note: Min, max: Minimum and maximum elongation (%) for the plate membranes
Freq: Frequency of the waveform (Hz)
DC: Duty cycle (%). The duty cycle is the percent of time that the waveform shape remains on at the rising part of the waveform.

As we observed that EC and VEC adhered very well to the membrane even after seeding for only two hours, we reduced the seeding time from 33.5 hours to 2.5 hours (**tab. 2**).

Table 2: Seeding program (short)

Step	Shape	Min	Max	Freq	DC %	Cycles	Duration
1	Static	0.0	15.0	1.0	50.0	9000	2.5 h
2	Static	0.0	13.0	1.0	50.0	6	6 sec
3	Static	0.0	11.0	1.0	50.0	6	6 sec
4	Static	0.0	9.0	1.0	50.0	6	6 sec
5	Static	0.0	7.0	1.0	50.0	6	6 sec
6	Static	0.0	5.0	1.0	50.0	6	6 sec
7	Static	0.0	3.0	1.0	50.0	6	6 sec
8	Static	0.0	1.0	1.0	50.0	6	6 sec

Note: Min, max: Minimum and maximum elongation (%) for the plate membranes
Freq: Frequency of the waveform (Hz)
DC: Duty cycle (%). The duty cycle is the percent of time that the waveform shape remains on at the rising part of the waveform.

After the seeding period, the cells were inspected under the microscope to make sure the cells were attached to the BioFlex Membrane and added 2 ml of cultivation media. Again, a part of the cells was additionally supplemented with 4 % CM1, a part with 4 % CM2 and a part with cultivation media exclusively. The BioFlex Cell Seeders were exchanged for BioFlex Loading Stations and the cells were subjected to a cyclic stretch **(tab. 3 + fig.13)** in the FlexCell FX-5000^{TM} device. Control cells, also with and without CM1 and CM2, were seeded on 6-well plates but not subjected to stretch.

Table 3: Stretching program

Step	Shape	Min	Max	Freq	DC	Cycles	Duration
1	Heart	0.0	0.1	1.0	50.0	300	5 min
2	Heart	0.0	0.2	1.0	50.0	300	5 min
3	Heart	0.0	0.4	1.0	50.0	300	5 min
4	Heart	0.0	0.6	1.0	50.0	300	5 min
5	Heart	0.0	0.8	1.0	50.0	43200	12 h
6	Heart	0.0	0.8	1.0	50.0	43200	12 h
7	Heart	0.0	0.8	1.0	50.0	43200	12 h
8	Heart	0.0	0.8	1.0	50.0	43200	12 h
9	Heart	0.0	0.8	1.0	50.0	43200	12 h
10	Heart	0.0	0.8	1.0	50.0	43200	12 h
11	Heart	0.0	0.6	1.0	50.0	300	5 min
12	Heart	0.0	0.4	1.0	50.0	300	5 min
13	Heart	0.0	0.2	1.0	50.0	300	5 min
14	Heart	0.0	0.1	1.0	50.0	300	5 min

Note: Min, max: Minimum and maximum elongation (%) for the plate membranes
Freq: Frequency of the waveform (Hz)
DC: Duty cycle (%). The duty cycle describes the time in percent of an active signal. Here the waveform shape remains at the rising part of the waveform on the time.

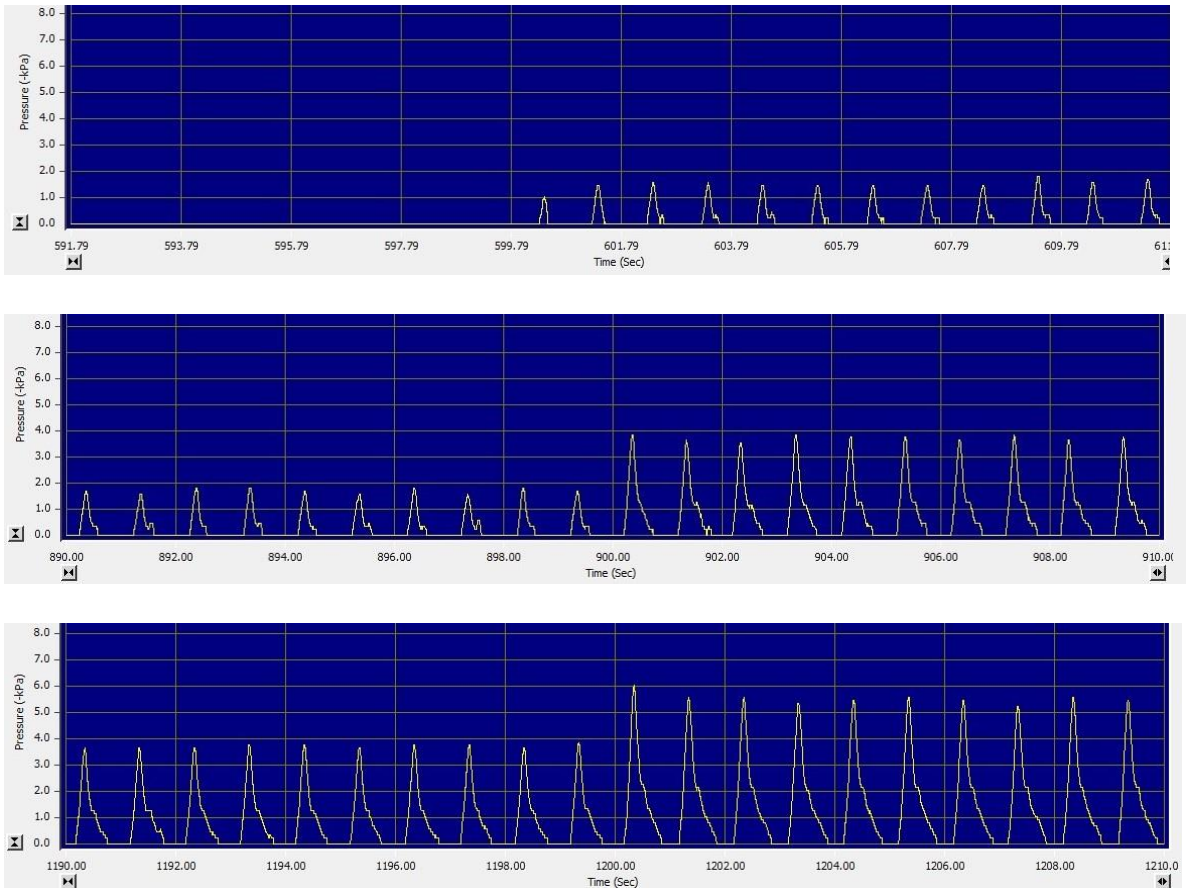

Figure 13 Graphical demonstration of the stretching program,
X-axis: time in seconds, Y-axis: pressure in kPa

3.4. Analysis on RNA level

3.4.1. Isolation of total RNA from cells

Isolation of RNA from cells was performed using the FavorPrep^{TM} Tissue Total RNA Kit (FavorGene Biotech Copr., Taiwan). The culture medium was aspirated, and the cells were washed once with PBS. The cells were then detached with 1x trypsin/EDTA solution and pelleted by centrifugation for 8 minutes at 1200 rpm at RT. The supernatant was completely removed and 350 µl of lysis buffer (consisting of buffer FARB and 1 % ß-mercaptoethanol) was added. To lyse the cells, the cell pellet was first mixed well with the buffer and homogenized over a filter column by centrifugation at 14 000 rpm for two minutes at RT. To the homogenized lysate, 350 µl of 70 % alcohol was added and mixed well. The sample was applied to a filter column located in a centrifuge tube and centrifuged at 14000 rpm for 1 minute. Then, 700 µl of wash buffer 1 was applied to the column and centrifuged at 14000 rpm for 1 minute at RT to wash the column. The column was transferred to a new centrifuge tube and 500 µl of wash buffer 2 was applied. Again, centrifugation was performed at 14000 rpm for 1 min at RT to wash the column. A second time, wash buffer 2 was applied and centrifuged at 14000 rpm for 2 min at RT to wash and dry the column. The column was transferred to a new centrifuge tube and DEPC (diethyl pyrocarbonate, Sigma, USA) treated water was applied. The column was run for 1 minute at 14000 rpm at RT centrifuged to release the RNA from the column. The RNA obtained was frozen at -80 °C.

3.4.2. Quantification of RNA (according to Maniatis, 1982)

The content of total RNA was quantified in aqueous solution by photometric absorbance measurement at a wavelength of 260 nm and 280 nm. An absorbance value of 1 corresponds to 40 µg/ml RNA (A260 = 1 = 40 µg/ml). The OD260/OD280 ratio provides information about the purity of the RNA preparation.

The calculation was performed according to the following scheme:

RNA content in µg = measured absorbance x dilution factor x 40 x volume.

3.4.3. Synthesis of complementary DNA (cDNA)

The cDNA synthesis was performed using "High-Capacity cDNA Reverse Transcription Kit" (ABI, USA). In this process, the isolated total RNA was transcribed into complementary DNA (cDNA) using with the use of the random primers for messenger RNA (mRNA), reaction buffer, deoxynucleotide mix (dNTP mix) and with an "MultiScribe™ Reverse Transcriptase.

A master mix consisting of the following reagents was prepared: 2 µl 10x reaction buffer, 0.8 µl dNTP mix (100 mM), 2 µl Random primer and 1 µl MultiScribe reverse transcriptase. This mixture was mixed gently and centrifuged briefly. The reagents were made up with H_2O to a total volume of 20 µl per reaction. Then, the corresponding amount of total RNA (1 µg) was added. The mixture was incubated for 10 minutes at +25 °C to allow the Random primer to bind to the RNA. This was followed by a two hour incubation at +37 °C. To denature the reverse transcriptase, incubation was at +85 °C for 5 seconds. After briefly cooling for 10 minutes to +4 °C, the synthesized cDNA could be used for real time (RT)-PCR. The remaining total RNA was also stored again at -80 °C.

3.4.4. Real-time quantitative polymerase chain reaction (RT-qPCR)

qPCRs were performed to analyze and identify gene expression patterns associated with stretch and calcification.

For qPCR, the kit “GoTaq qPCR Master Mix” from the company Promega was used.
The qPCR-mastermix consisted of the GoTaq qPCR Master Mix - which includes dsDNA-binding dye, carboxy-X-rhodamine (CXR) reference dye, GoTaq Hot Start Polymerase, $MgCl_2$, dNTPs and a reaction buffer - a forward and a reverse primer **(tab. 5)** and nuclease-free water **(tab. 4).**

Table 4: qPCR-Mastermix for one reaction (RT-qPCR)

Reagent	Volume
GoTaq qPCR Master Mix	12.5 µl
Primer F [10 pmol]	2.5 µl
Primer R [10 pmol]	2.5 µl
Nuclease-free water	2.5 µl
Summed	**20.0 µl**

Table 5: Primer sequences (RT-qPCR)

Name	Primer 5' – 3'	Tm	Sequence	Product	Company	Acc. Nr.
GAPDH pig forward	CAG GTT GTG TCC TGT GAC TTC	61.2 °C	932-952	89 bp	Microsynth	NM_001206359.1
GAPDH pig reverse	TTG ACG AAG TGG TCG TTG AG	58.4 °C	1020-1001	89 bp	Microsynth	NM_001206359.1
YAP pig forward	CAG AAC CGT TTC CCA GAC TAT C	62.1 °C	1020-1001	103 bp	Microsynth	XM_013979322.1
YAP pig reverse	GCA TCA ACT CCT CTC CTT CTA TG	62.9 °C	1981-1959	103 bp	Microsynth	XM_013979322.1
TAZ1 pig forward	CCA GCA GGG CTC ATG AAT ATG	61.2 °C	664-684	107 bp	Microsynth	XM_013992351.1
TAZ1 pig reverse	CGC ATC CTA ATC CTC TCT CTC T	62.1 °C	770-749	107 bp	Microsynth	XM_013992351.1
OPG pig forward	CCT GTC CTG ACC ACT ATT ACA C	61.7 °C	120-142	106 bp	Microsynth	EF543195
OPG pig reverse	CGA TTG CAT TCC TGC TTG AC	61.7 °C	225-205	106 bp	Microsynth	EF543195
OPN pig forward	CCC ATC TCA GAA GCA GAC TTT C	62.1 °C	238-259	107 bp	Microsynth	NM_214023.1
OPN pig reverse	CAG GGC TTT CGT TGG ACT TG	60.5 °C	344-325	107 bp	Microsynth	NM_214023.1

The cDNA synthesized the previous day, was diluted 1:4 with nuclease-free water. 5 µl of RNA were used for each well of the PCR plate and 20 µl of qPCR Mastermix was added. Each sample was pipetted as a triplet and each qPCR run was repeated three times. The plate was carefully sealed with an adhesive film, centrifuged to spin down the samples, and put into a 7500 Real-Time PCR cycler (Applied Biosystems, **tab.6)**.

The relative quantification method (ΔΔ CT) was used to analyze relative mRNA expression. After outliners were excluded manually, mean cycle threshold (CT) values and standard deviations (SD) were calculated using the program Excel. Furthermore, Δ CT values, showing the difference between calculated CT-means of genes of interest and the endogenous control gene (GAPDH), and ΔΔ CT values, demonstrating the difference between Δ CT values of cells treated with calcification medium (CM1/2) and Δ CT values of corresponding untreated cells, were calculated. To facilitate comparison of data, the fold change of the mRNA expression was calculated. A positive fold change indicates an upregulation of the gene, while a negative fold change indicates a downregulation.
The calculated data was statistically analyzed and visualized with the software "GraphPad Prism9", using a One-way ANOVA and Bonferroni's multiple comparisons test to identify significant differences.

Table 6: Cycler program (7500 Real Time PCR)

	Temperature	**Time**
Holding stage	50 °C	2 min
	95 °C	10 min
Cycling stage (40 cycles)	95 °C	15 sec
	62 °C	1 min
Melt curve stage	95 °C	15 sec
	60 °C	1 min
	95 °C	30 sec
	60 °C	15 sec

3.5. Analysis on protein level

3.5.1. Protein extraction from cells

A 80 cm² culture flask (approximately 1.5 x 10^6 cells) densely covered with cells was used for protein isolation in each case. The culture medium was aspirated, the cells washed once with PBS, detached from the flask with a cell scraper (Corning, USA), and transferred to a centrifuge tube with 400 µl PBS. After centrifugation at 1200 rpm for 5 minutes at RT, the supernatant was removed and the cells were dissolved in an appropriate volume of extraction buffer (20 mM Tris, 137 mM NaCl, 10 % glycerol, 1 % NP-40, 10 mM EDTA and Complete Protease Inhibitor Cocktail (Roche Molecular Biochem., USA)). After incubation for 30 minutes on ice, the extract was centrifuged at 14000 rpm for 30 minutes at +4 °C. The supernatant containing the cytosolic proteins was transferred to a new tube and stored at -80 °C.

3.5.2. Quantification of proteins (according to Bradford, 1976)

The determination of the total protein content of the extracts was performed using the Bio-Rad Protein Assay (Bio-Rad Laboratories, USA). For this purpose, a standard series was first prepared with a stock solution of BSA-V (0.1 mg/ml) stored portioned at -20 °C. Then, the protein extracts were diluted 1:400 with H_2O. The BSA standard series and protein extracts were then mixed with 200 µl of the Bio-Rad dye solution and measured in a photometer at a wavelength of 595 nm after incubation for 10 minutes at RT. An optical density (OD) value of 0.1 corresponds - in the linear range - to a protein content of approximately 1 µg.

3.5.3. Electrophoretic separation of proteins

Separation of proteins by molecular weight was performed in 10 % polyacrylamide gels. First, the separation gel consisting of acrylamide/bis solution (30 %) (Serva, Germany), 1.5 M Tris pH=8.8, H_2O, 10 % sodium dodecyl sulfate (SDS), and 10 % ammonium persulfate (APS) was mixed (all substances Sigma, USA, **tab. 7)**. After addition of N,N,N',N'-tetramethylenediamine (TEMED) as polymerization initiator, the acrylamide solution was introduced into the gel apparatus and overlaid with isopropanol. After a polymerization time of 1 hour at RT, the isopropanol was removed, the gel was washed with water, and the collecting gel **(tab. 8)** was poured onto the separating gel. For this purpose, arylamide/bis solution (30 %), 0.5 M Tris pH=6.8, H2O, 10 % APS, 10 % SDS and TEMED were mixed and carefully applied. The comb was introduced without air bubbles. After a polymerization time of 45 min at RT, the comb was carefully removed under 1x running buffer (25 mM Tris, 190 mM glycine, 1 % SDS) and the resulting slots were carefully rinsed with a pipette after the gel was fixed in the running buffer chamber. For protein gel electrophoresis, 30 µg protein/gel pocket was applied. For this purpose, the corresponding protein extract volume was mixed with the same volume of 6x sample buffer (12 % 60 mM Tris pH=6.8, 12 % SDS, 9.3 % dichlorodiphenyltrichloroethane (DDT), 0.06 % bromophenol blue, 47 % glycerol, H_2O) and mixed well. After the denaturation at 95 °C for 5 minutes, protein extracts were briefly centrifuged and pipetted into gel pockets. The molecular weight standard used was the Prestained Protein Standard™, a pre-stained molecular weight standard (Bio-Rad Laboratories, USA).

Discontinuous gel electrophoresis was performed at 40 volts for 1 hour, then at 60 volts for 4 hours using the mini-apparatus (Bio-Rad Laboratories, USA).

Table 7: Composition of the Separation Gel

Separation gel	**10 %**
Acrylamide/bis-Solutioin	4000 µl
1.5 M Tris pH=8.8	3000 µl
ddH_2O	4880 µl
10 % APS	80 µl
10 % SDS	120 µl
TEMED	8 µl

Table 8: Composition of the Collection Gel

Collecting Gel	
Acrylamide/bis-Solutioin	625 µl
1.5 M Tris pH=8.8	925 µl
ddH_2O	2125 µl
10 % APS	50 µl
10 % SDS	37.5 µl
TEMED	2.5 µl

3.5.4. Immunoblot Analysis

The resulting gel was transferred onto a polyvinylidene difluoride (PVDF) membrane (Millipore, Bedford, USA) by tank blotting.

The membranes were blocked with 1x Tris-buffered saline (TBS), 0.1 % (v/v) Tween 20 (TBST) containing 5 % non-fat dry milk for one hour at RT and incubated over night at 4 °C with primary-antibody.

The antibodies used were as follows, YAP1 (rabbit, clone D8H1X, Cell Signaling Technology, USA), TAZ (rabbit, clone V386, Cell Signaling Technology, USA), OPN (mouse-anti-human, clone AKm2A1, Santa Cruz Biotechnology Inc., USA), OPG (mouse-anti-human, clone E-10, Santa Cruz Biotechnology Inc., USA) and as endogenous control anti-ß-actin (clone AC-15, Sigma, USA).

The membrane was washed with 1x TBS, 0.1 % (v/v) Tween 20 and incubated for 1 hour at RT with horseradish peroxidase (HRP) -conjugated anti-rabbit or anti-mouse secondary antibody (Dako, Austria) in 5 % (v/v) non-fat dry milk in 1 x TBS, 0.1 % (v/v) Tween 20. The immunoblots were developed using enhanced chemiluminescence (ECL) detection reagent (0.1 M TRIS pH=8.6; 13.07 mg/ml p-Coumaric acid, 0.044 mg/ml Luminol and 3 % H_2O_2). Blots were analysed with ChemiDoc™ XRS system (BioRad, Austria).

4. Results

4.1. Immunofluorescence staining

Cells were analyzed by immunofluorescence staining to verify their characterization. EC and VEC showed positive signals for Von Willebrand factor (VWF) and CD31 (**fig. 14+15**), both of which are markers for endothelial cells. Weak signals of smooth muscle actin (SMA, **fig. 16**) were detected and could be visualized by drastically increasing the exposure time. Smooth muscle actin is a marker that is characteristic of intestinal cells. Image processing using the "Nucance2.8.0." software was performed. Adequate scale bars indicating 100 µm were applied using the "Image J" software. The stainings were recorded at 400x magnification.

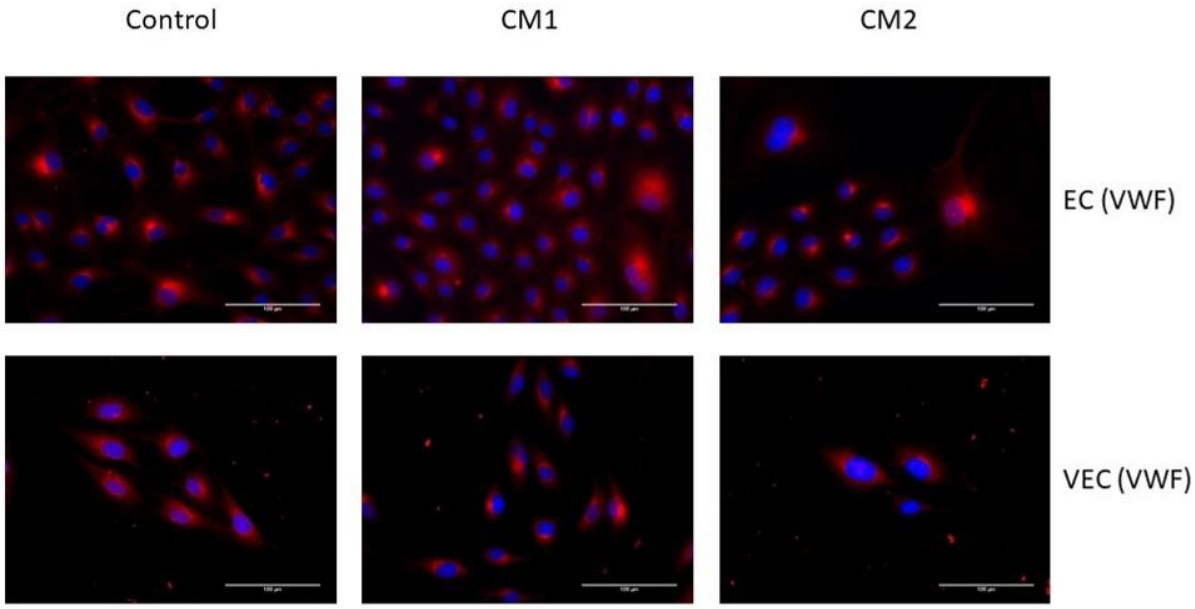

Figure 14 Immunofluorescence analysis of EC and VEC with primary antibody Von Willebrand Factor (red) and DAPI (blue) as control staining. Scale bars indicate 100 µm.

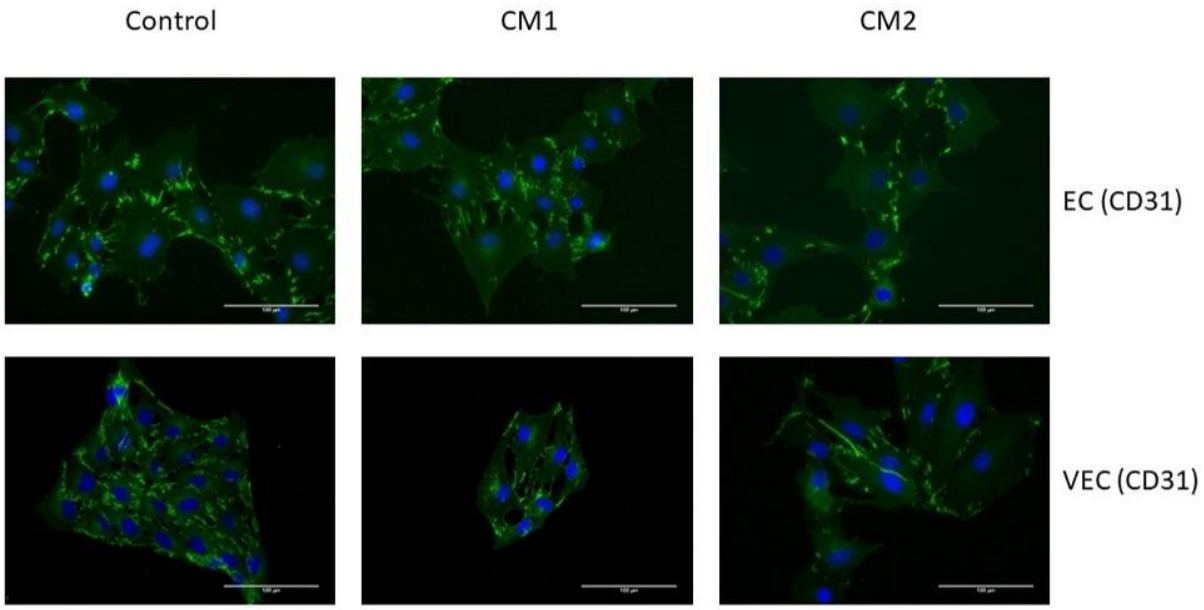

Figure 15 Immunofluorescence analysis of EC and VEC with primary antibody CD31 (green) and DAPI (blue) as control staining. Scale bars indicate 100 µm.

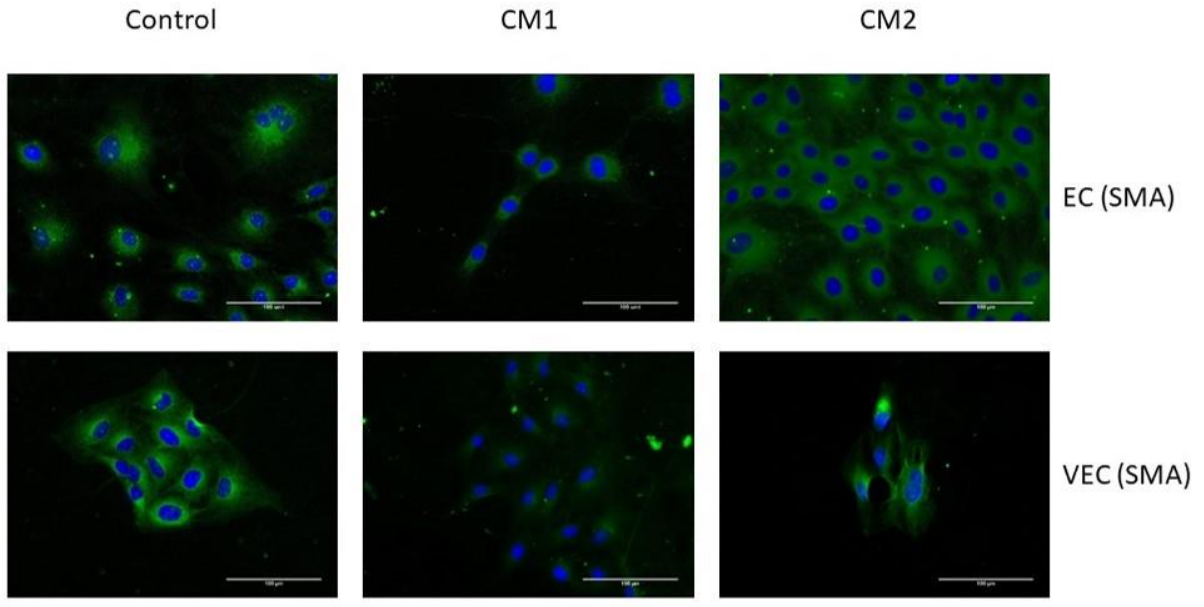

Figure 16 Immunofluorescence analysis of EC and VEC with primary antibody smooth muscle actin (SMA, green) and DAPI (blue) as control staining. Scale bars indicate 100 µm.

4.2. Alizarin Red Staining

To verify and compare the calcification-inducing effect of the two calcification media (CM1 and CM2), Alizarin Red staining was performed **(tab. 9)** allowing hydroxyapatite deposition to be measured.

Table 9: Mean values and standard deviation of photometric density measurement at 405 nm wavelength after Alizarin Red Staining of vascular endothelial cells, treated with CM1 or CM2 and untreated cells. Outliers marked for statistical analysis were highlighted.

Sample	CO		CM1		CM2	
	Mean	SD	Mean	SD	Mean	SD
1	0.04	0.00047	0.08	0.00022	0.13	0.00356
2	0.04	0.00047	0.07	0.00027	0.06	0.00069
3	0.05	0.00054	0.06	0.00090	0.06	0.00130
4	0.05	0.00051	0.05	0.00043	0.09	0.00272
5	0.11	0.00207	0.08	0.00203	0.07	0.00206
6	0.05	0.00104	0.13	0.00347	0.07	0.00139
7	0.05	0.00081	0.06	0.00024	0.05	0.00025
8	0.04	0.00034	0.09	0.00252	0.05	0.00044

The measurements show an increased photometric density at a wavelength of 405 nm after treatment of CM1 or CM2. The relative photometric density of the measurements with CM1, as well as CM2 are significantly increased ($P < 0.0001$), compared with the untreated control, with CM1 significantly higher than CM2 ($P < 0.001$; **fig.17**).

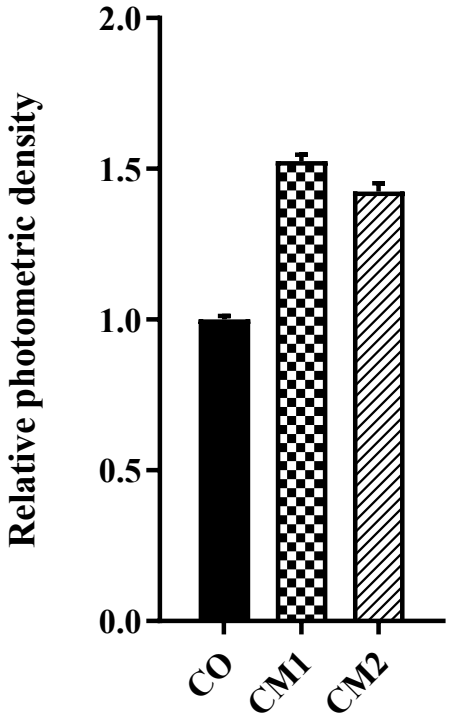

Figure 17 Mean and standard deviation of relative photometric density (wavelength: 405 nm) of Alizarin Red Staining from vascular endothelial cells, treated with CM1 or CM2 for five weeks.

4.3. qPCR

After RNA isolation and cDNA synthesis, qPCRs were performed to analyze and identify gene expression patterns associated with stretch and calcification. Data were obtained from independent experiments, in which each condition was carried out three times and every sample was pipetted thrice **(tab. 10-13)**.

Table 10: Mean values and standard deviation of Ct and **Δ** Ct, **ΔΔ Ct** and x-fold (ratio) data after analysis of GAPDH, YAP, TAZ, OPN, and OPG in unstretched vascular endothelial cells with qPCR.

EC CO non-stretched						
	Mean (Ct)	**SD (Ct)**	**Δ Ct**	**ΔΔ Ct**	**Ratio**	**SD (Δ Ct)**
GAPDH	19.24	0.65	-	-	-	-
YAP	24.97	0.41	5.72	-	1.00	0.77
TAZ	22.74	0.28	3.50	-	1.00	0.71
OPG	27.47	1.16	8.23	-	1.00	1.33
OPN	26.07	0.33	6.83	-	1.00	0.73
EC CM1 non-stretched						
	Mean (Ct)	**SD (Ct)**	**Δ Ct**	**ΔΔ Ct**	**Ratio**	**SD (Δ Ct)**
GAPDH	18.66	0.67	-	-	-	-
YAP	24.19	1.14	5.53	-0.19	0.88	1.32
TAZ	22.85	1.30	4.19	0.69	1.62	1.46
OPG	27.67	1.13	9.02	0.79	1.73	1.31
OPN	25.58	0.74	6.93	0.10	1.07	1.00
EC CM2 non-stretched						
	Mean (Ct)	**SD (Ct)**	**Δ Ct**	**ΔΔ Ct**	**Ratio**	**SD (Δ Ct)**
GAPDH	19.07	1.23	-	-	-	-
YAP	25.20	1.23	6.14	0.41	1.33	1.74
TAZ	23.02	1.10	3.95	0.45	1.37	1.65
OPG	27.45	1.30	8.39	0.16	1.12	1.79
OPN	24.26	2.42	5.19	-1.63	0.32	2.72

Table 11: Mean values and standard deviation of Ct and **Δ** Ct, **ΔΔ Ct** and x-fold (ratio) data after analysis of GAPDH, YAP, TAZ, OPN, and OPG in stretched vascular endothelial cells with qPCR.

EC CO stretched						
	Mean (Ct)	**SD (Ct)**	**Δ Ct**	**ΔΔ Ct**	**Ratio**	**SD (Δ Ct)**
GAPDH	20.55	2.42	-	-	-	-
YAP	23.42	0.41	2.87	-	1.00	2.45
TAZ	21.65	0.34	1.10	-	1.00	2.44
OPG	26.04	0.73	5.49	-	1.00	2.52
OPN	25.46	0.51	4.90	-	1.00	2.47
EC CM1 stretched						
	Mean (Ct)	**SD (Ct)**	**Δ Ct**	**ΔΔ Ct**	**Ratio**	**SD (Δ Ct)**
GAPDH	18.96	1.04	-	-	-	-
YAP	24.22	0.56	5.26	2.38	5.22	1.18
TAZ	21.97	0.75	3.01	1.91	3.76	1.29
OPG	27.24	1.04	8.28	2.79	6.94	1.47
OPN	26.13	1.06	7.17	2.27	4.81	1.48
EC CM2 stretched						
	Mean (Ct)	**SD (Ct)**	**Δ Ct**	**ΔΔ Ct**	**Ratio**	**SD (Δ Ct)**
GAPDH	20.02	1.79	-	-	-	-
YAP	24.44	1.43	4.42	1.55	2.93	2.29
TAZ	22.86	1.04	2.84	1.74	3.35	2.07
OPG	29.18	0.49	9.16	3.68	12.79	1.86
OPN	25.98	0.93	5.96	1.06	2.09	2.02

Table 12: Mean values and standard deviation of Ct and **Δ** Ct, **ΔΔ Ct** and x-fold (ratio) data after analysis of GAPDH, YAP, TAZ, OPN, and OPG in unstretched valvular endothelial cells with qPCR.

VEC CO non-stretched						
	Mean (Ct)	**SD (Ct)**	**Δ Ct**	**ΔΔ Ct**	**Ratio**	**SD (Δ Ct)**
GAPDH	17.93	0.76	-	-	-	-
YAP	22.46	0.15	7.36	-	1.00	0.77
TAZ	22.06	1.24	6.96	-	1.00	1.45
OPG	25.70	0.93	10.60	-	1.00	1.20
OPN	22.85	0.85	7.75	-	1.00	1.14
VEC CM1 non-stretched						
	Mean (Ct)	**SD (Ct)**	**Δ Ct**	**ΔΔ Ct**	**Ratio**	**SD (Δ Ct)**
GAPDH	17.35	0.48	-	-	-	-
YAP	22.84	0.83	5.49	-1.87	0.27	0.96
TAZ	21.27	0.42	3.92	-3.04	0.12	0.64
OPG	25.29	0.55	7.95	-2.66	0.16	0.73
OPN	23.74	1.16	6.40	-1.35	0.39	1.26
VEC CM2 non-stretched						
	Mean (Ct)	**SD (Ct)**	**Δ Ct**	**ΔΔ Ct**	**Ratio**	**SD (Δ Ct)**
GAPDH	20.26	0.32	-	-	-	-
YAP	23.90	0.81	3.64	-3.72	0.08	0.87
TAZ	22.52	0.47	2.26	-4.70	0.04	0.57
OPG	25.75	0.81	5.49	-5.11	0.03	0.87
OPN	23.32	0.40	3.06	-4.70	0.04	0.51

Table 13: Mean values and standard deviation of Ct and **Δ** Ct, **ΔΔ Ct** and x-fold (ratio) data after analysis of GAPDH, YAP, TAZ, OPN, and OPG in stretched vascular endothelial cells with qPCR.

VEC CO stretched						
	Mean (Ct)	**SD (Ct)**	**Δ Ct**	**ΔΔ Ct**	**Ratio**	**SD (Δ Ct)**
GAPDH	19.79	0.14	-	-	-	-
YAP	24.05	0.98	4.26	-	1.00	0.99
TAZ	22.48	0.18	2.69	-	1.00	0.23
OPG	26.10	0.26	6.31	-	1.00	0.30
OPN	24.34	0.45	4.55	-	1.00	0.47
VEC CM1 stretched						
	Mean (Ct)	**SD (Ct)**	**Δ Ct**	**ΔΔ Ct**	**Ratio**	**SD (Δ Ct)**
GAPDH	19.84	0.12	-	-	-	-
YAP	25.01	0.08	5.17	0.91	1.88	0.14
TAZ	22.35	0.55	2.51	-0.18	0.88	0.56
OPG	27.68	0.30	7.84	1.53	2.88	0.32
OPN	24.77	0.18	4.93	0.38	1.31	0.21
VEC CM2 stretched						
	Mean (Ct)	**SD (Ct)**	**Δ Ct**	**ΔΔ Ct**	**Ratio**	**SD (Δ Ct)**
GAPDH	19.35	1.39	-	-	-	-
YAP	24.80	1.67	5.45	1.19	2.29	2.17
TAZ	22.40	0.49	3.05	0.36	1.29	1.47
OPG	27.76	1.58	8.41	2.10	4.28	2.10
OPN	23.85	0.13	4.50	-0.05	0.97	1.40

4.3.1. Vascular endothelial cells

In vascular endothelial cells, mechanical strain resulted in an increase of mRNA expression of YAP, TAZ, OPG, and OPN. Whereas in YAP, TAZ, and OPN, calcification medium with inorganic phosphate, CM1, lead to elevated expression of mRNA; in OPG, mRNA expression increased most by the addition of CM2, the calcification medium with organic phosphate **(Fig. 18).**

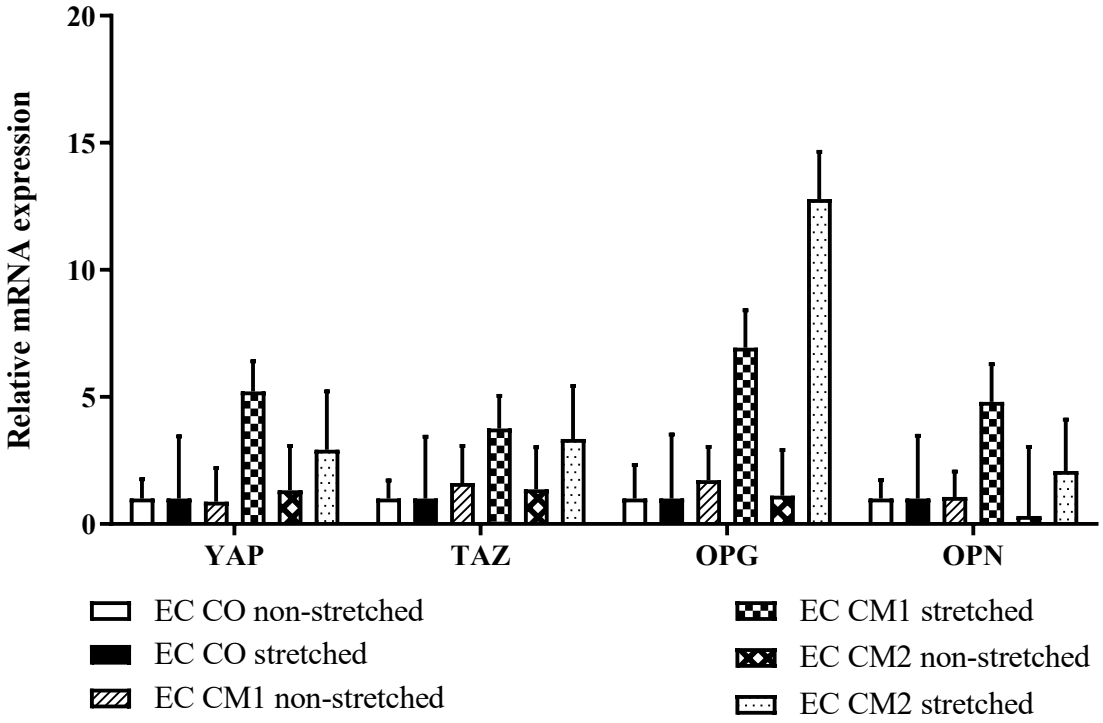

Figure 18 mRNA expression data from stretched and unstretched vascular endothelial cells, with and without the addition of calcification medium.

While the expression of YAP **(fig. 19)** in unstretched vascular endothelial cells was slightly different between control group, CM1 and CM2, in stretched vascular endothelial cells an increase (P value = 0.0007) of mRNA expression of YAP was observed when treated with CM1. In unstretched endothelial cells, mRNA expression of TAZ **(fig. 20**) was slightly increased by the addition of calcification media. In the corresponding stretched cells, an increase in TAZ expression was detected (CM1: 5.22-fold ± 1.18; compared to CO).

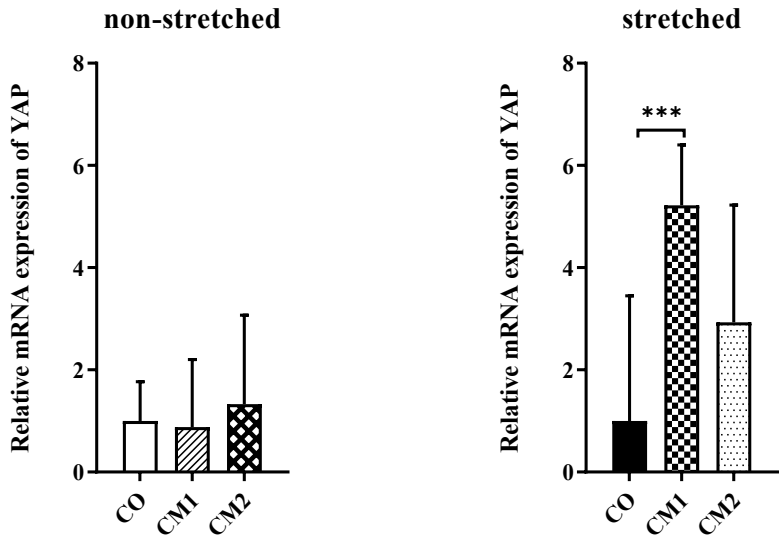

Figure 19 mRNA expression data of YAP from stretched and unstretched vascular endothelial cells, with and without the addition of calcification medium, ***P < 0.001.

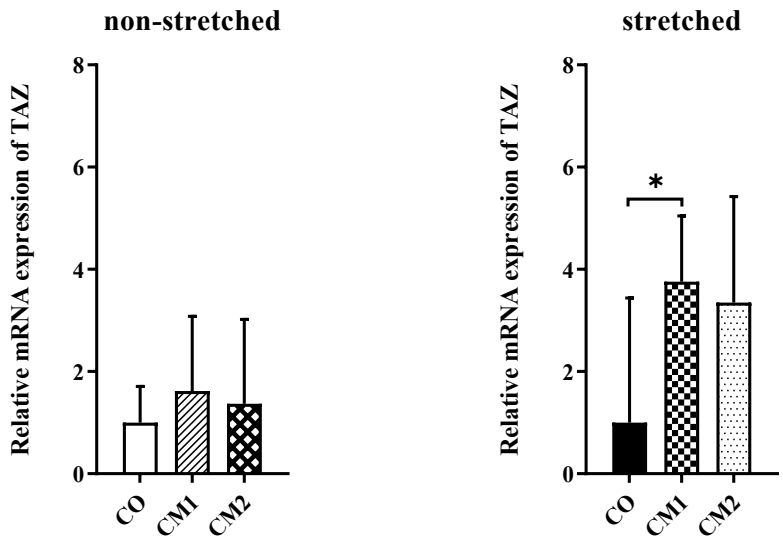

Figure 20 mRNA expression data of TAZ from stretched and unstretched vascular endothelial cells, with and without the addition of calcification medium, *P < 0.05.

In stretched vascular endothelial cells, treatment with CM1 and CM2 significantly increased the mRNA expression of OPG (CM1: 6.94-fold ± 1.47; CM2: 12.79-fold ± 1.86; P < 0.0001), whereas in unstretched cells no significant changes were observed **(fig. 21)**. Treatment with CM1 in stretched vascular endothelial cells increased the expression of OPN (P < 0.01), compared to stretched control cells. In unstretched cells, no significant changes were detected between CO, CM1, and CM2 **(fig. 22).**

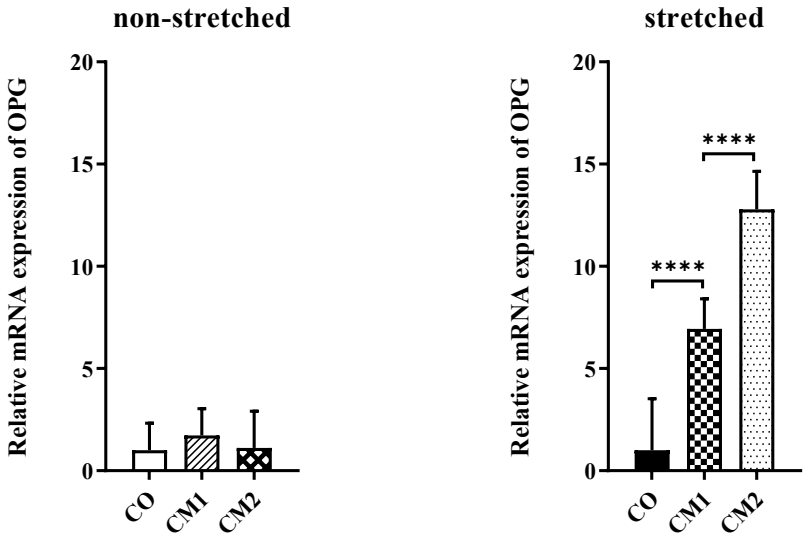

Figure 21 mRNA expression data of OPG from stretched and unstretched vascular endothelial cells, with and without the addition of calcification medium, ****P < 0.0001.

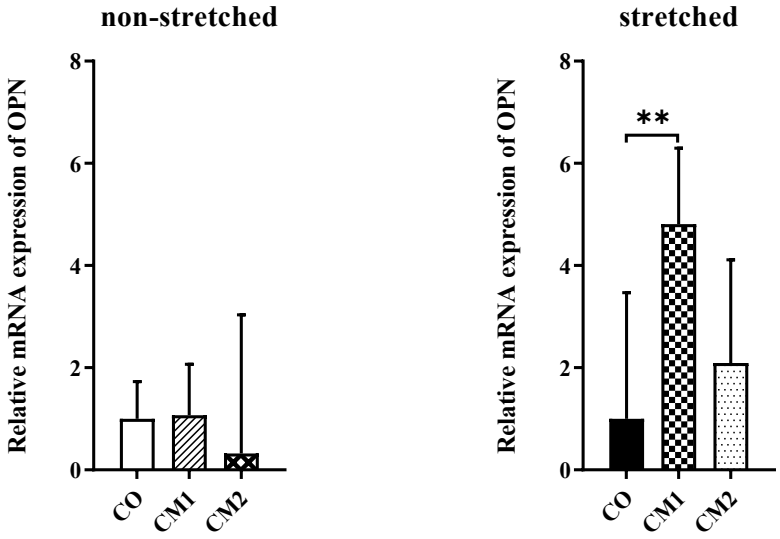

Figure 22 mRNA expression data of OPN from stretched and unstretched vascular endothelial cells, with and without the addition of calcification medium, **P < 0.01.

4.3.2. Vavlular endothelial cells

The analyzed mRNA expressions of VEC showed a quite inhomogeneous pattern. The expressions of YAP, TAZ, OPN, and OPG tended to be increased in stretched cells, treated with CM1 or CM2. Unstretched and CM2-treated cells showed decreased mRNA expression of YAP, TAZ, OPN, and OPG **(fig. 23).**

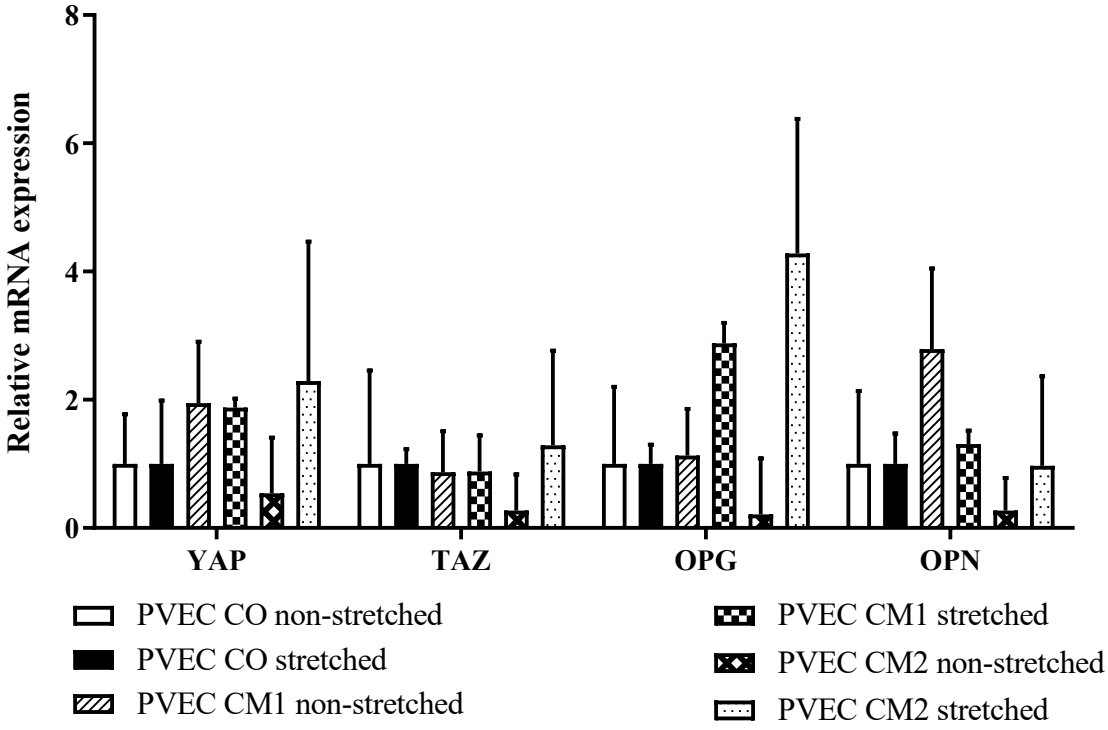

Figure 23 mRNA expression data from stretched and unstretched valvular endothelial cells, with and without the addition of calcification medium.

In unstretched valvular endothelial cells, treatment of CM2 resulted in decreased mRNA expression of YAP, compared to cells treated with CM1 (CM2: 0.54-fold ± 0.87; compared to CM1: 1.95-fold ± 0.96; P value = 0.0083). In the corresponding stretched cells, no significant variations were detected between CM1, CM2, and the control group **(fig. 24)**. Neither mechanical stress, nor the addition of CM1 or CM2 altered the expression of TAZ in valvular endothelial cells **(fig. 25)**.

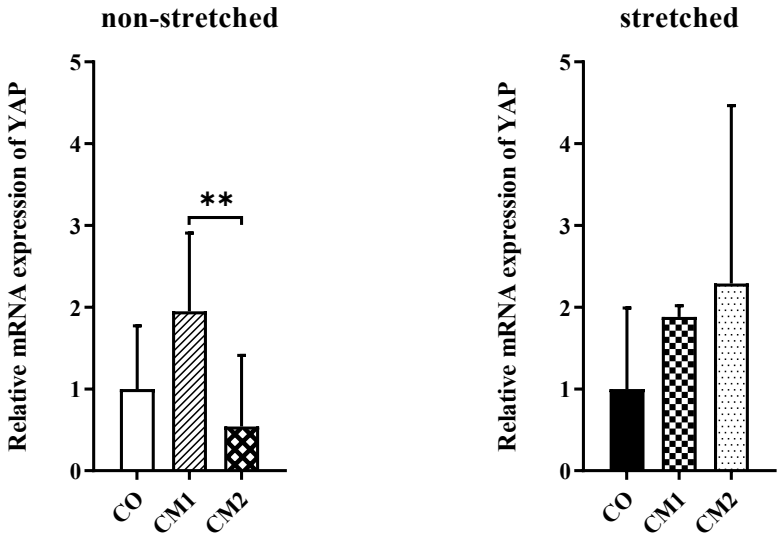

Figure 24 mRNA expression data of YAP from stretched and unstretched valvular endothelial cells, with and without the addition of calcification medium, **P < 0.01.

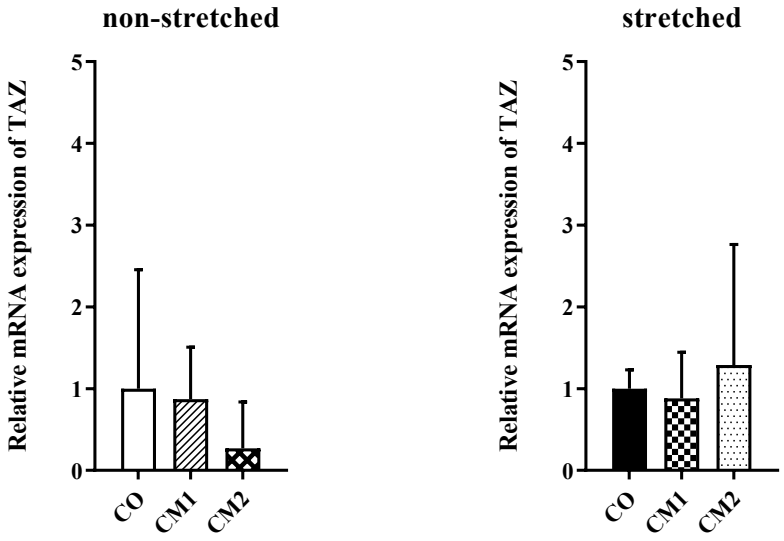

Figure 25 mRNA expression data of TAZ from stretched and unstretched valvular endothelial cells, with and without the addition of calcification medium.

In stretched valvular endothelial cells, treatment with CM2, increased the expression of OPG (4.28-fold ± 2.10, P = 0.0011), compared with stretched but non-treated cells **(fig. 26)**. In the corresponding unstretched cells, no strong variations could be detected between CM1, CM2, and the control group. In unstretched valvular endothelial cells, addition of CM1 increased mRNA expression of OPN, whereas addition of CM2 decreased OPN expression (CM1: 2.79-fold ± 1.26; CM2: 0.27-fold ± 0.51) compared to control cells **(fig. 27)**.

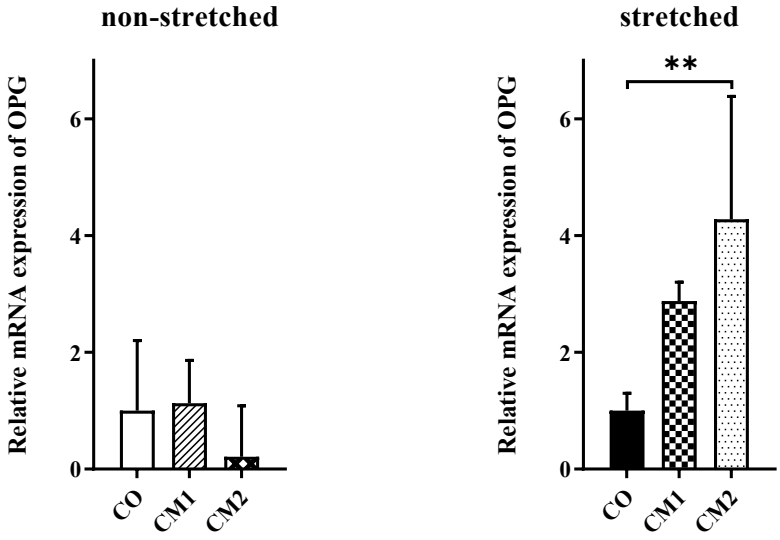

Figure 26 mRNA expression data of OPG from stretched and unstretched valvular endothelial cells, with and without the addition of calcification medium, **P < 0.01

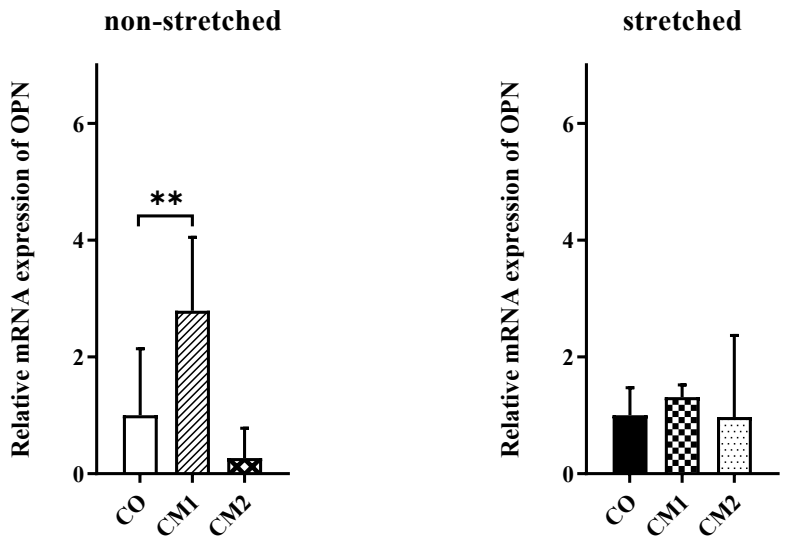

Figure 27 mRNA expression data of OPN from stretched and unstretched valvular endothelial cells, with and without the addition of calcification medium, **P < 0.01

4.4. Western blots

Western blots were performed to analyze the protein expression of YAP, TAZ, OPN, and OPG **(fig. 28-30)**. ß-actin served as a control. Protein isolates from vascular and valvular endothelial cells were used to compare protein expression of YAP, TAZ, OPN, and OPG, stretched and unstretched, and with and without CM1/2. The intensity of the bands of each protein was determined using the software "ChemiDoc – Quantity One" and the ratio of the protein of interest to the reference protein was visualized using a bar diagram.

In vascular endothelial cells (EC), mechanical stress and the addition of CM1/2 decrease the expression of YAP, while in VEC, in the unstretched samples, the expression of YAP increases through the addition of CM1/2. However, the combination of CM1 or CM2 and mechanical stress in VEC leads to a decrease in the protein expression of YAP **(fig. 28)**.

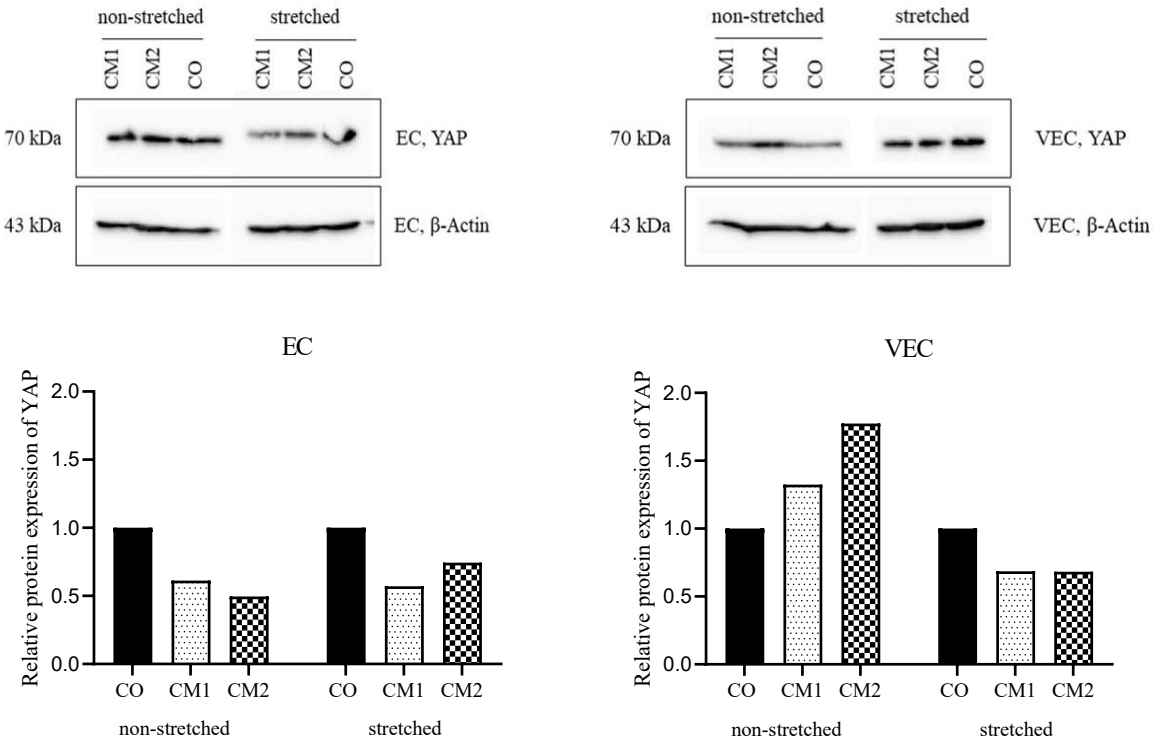

Figure 28 Expression of YAP determined using Western blots, with and without mechanical stress, with and without CM1/2, in EC and VEC.

In EC and VEC, mechanical stress and the addition of calcification medium lead to a decreased protein expression of TAZ **(fig. 29)**. The unstretched samples, cultivated with CM2, show an increase in the expression of TAZ. Unstretched VEC and EC show variations in terms of protein expression of TAZ by the addition of CM1, which is reduced in the vascular endothelial cells, whereas it is slightly increased in samples of valvular endothelial cells.

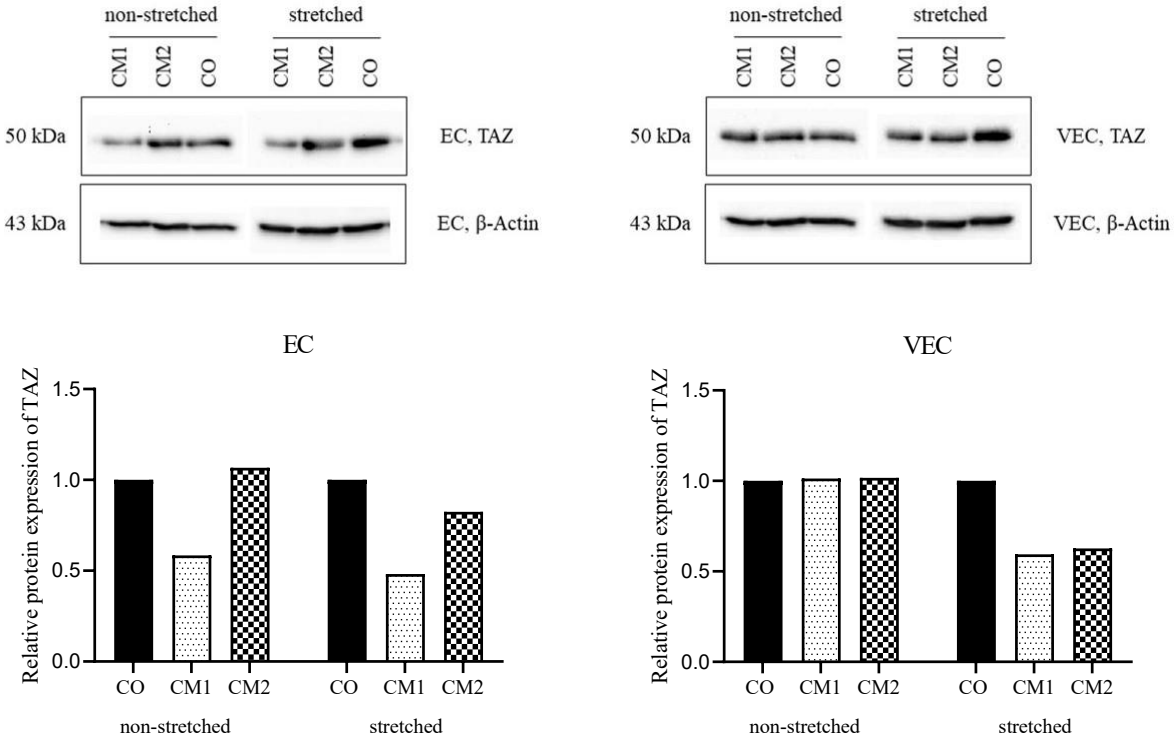

Figure 29 Expression of TAZ determined using Western blots, with and without mechanical stress, with and without CM1/2, in EC and VEC.

Neither OPN nor OPG could be detected, although there was a clear signal for the endogenous control, ß-Actin **(fig. 30)**.

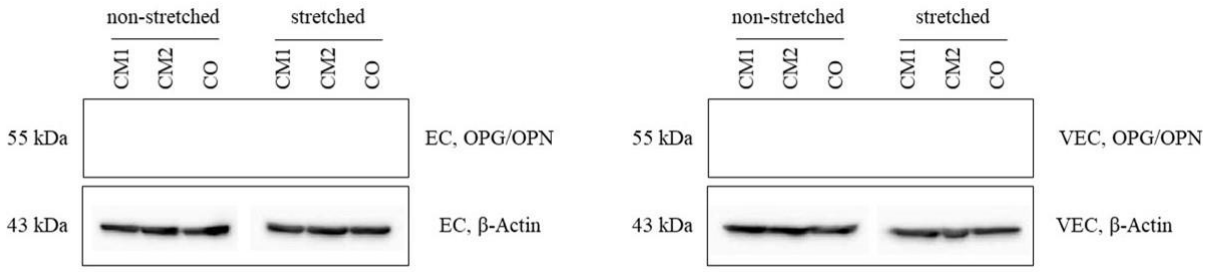

Figure 30 Expression of OPN/OPG determined using Western blots, with and without mechanical stress, with and without CM1/2, in EC and VEC.

5. Discussion

In this bachelor thesis, I investigated the influence of mechanical strain and calcification on porcine vascular endothelial cells (EC) and porcine valvular endothelial cells (VEC) *in vitro* and analyzed the involved molecular mechanisms. I focused on the expression patterns of the calcification-related genes *YAP*, *TAZ*, *OPG*, and *OPN*.

For this purpose, it was necessary to evaluate the characterization of the isolated cells. It could be verified by immunofluorescence staining that EC and VEC show positive signals of Von Willebrand Factor (VWF) and platelet endothelial cell adhesion molecule-1 (CD31), representing markers for endothelial cells. In addition, Alizarin Red staining was performed, proving that both calcification media, the one with inorganic (CM1), and the one with the organic phosphate (CM2), produce deposits of hydroxyapatite in the cells (Gregory, et al. 2004).

After analyzing the qPCRs of EC, we observed that mechanical stress and treatment with calcification medium (CM1/2) increased the mRNA expression of YAP, TAZ, OPG, and OPN, compared to untreated, stretched, and unstretched control cells. Our results confirm data published by Rutkovskiy, *et al*. reporting that mechanical stress, imposed on endothelial cells, induces the expression of genes that are related to calcification (Rutkovskiy, et al. 2019). However, in VEC, we could not observe the same mRNA expression patterns, indicating that endothelial cells, isolated from the aorta behave differently in this manner from endothelial cells from cardiac valves.

For instance, on one hand, our qPCR data show highly increased mRNA expression of YAP in EC after mechanical stress and treatment with CM1, which not only leads to calcification but also triggers an immune reaction (Mathieu, et al. 2015).

On the other hand, not only in stretched but also in unstretched VEC treated with CM1, an increase in mRNA expression of YAP was detected. Treatment with CM2 resulted in increased mRNA expression of YAP in both, unstretched and stretched EC. In stretched VEC, we observed a similar mRNA expression pattern of YAP, but in unstretched VEC, treatment with CM2 lead to a decrease in mRNA expression of YAP.

Numerous articles reported that the Hippo signaling pathway is highly responsive to various stimuli, such as mechanical cues and inflammation (Piccolo, et al. 2014; Totaro, et al. 2018; Yu, et al. 2015; Zheng and Pan 2019). As YAP functions as a main transcriptional regulator of this pathway, this aspects support our data on the increased mRNA expression of YAP after mechanical stress and the addition of CM1. However, our corresponding protein data of stretched and unstretched EC showed that treatment with CM1 and CM2 decreased the protein expression of YAP. In stretched VEC, protein expression of YAP showed the same pattern as in EC. In contrast, in unstretched VEC, protein expression of YAP was increased by CM1 and CM2.

One explanation is that the calcification process was in its early stages - the expression of YAP was already increased on the mRNA level, but proteins were not yet synthesized in all cell groups. To confirm this, further approaches with prolonged addition of calcification medium would be needed.

Moreover, our data showed that both calcification media can upregulate the expression of TAZ on mRNA level in vascular endothelial cells, VEC, in contrast, showed a different gene expression. In unstretched VEC, a decrease in mRNA expression of TAZ after treatment with CM1 and CM2 was detected, whereas in stretched VEC, CM1 lead to a slight decrease, and CM2 to an increase in the mRNA expression of TAZ.

Comparing our qPCR data with our Western blot data, a different expression pattern of TAZ on protein level was observed. In stretched EC and VEC, treatment with CM1 and CM2 decreased the protein expression of TAZ, while unstretched EC and VEC showed a slightly increased protein expression of TAZ after treatment with CM2, allowing us to conclude that gene expression of TAZ is dependent on mechanical stress.

In literature, YAP and TAZ are mostly referred to as a unit in which YAP and TAZ are linked and function together (Meng, et al. 2016; Pocaterra and Romani 2020; Totaro, et al. 2018). Our mRNA and protein data showed that YAP and TAZ behaved only partially the same, suggesting that they do not always act in linked condition. This was further demonstrated by data published by Kim, *et al.* and Neto, *et al.,* reporting that YAP and TAZ not only have different expressions, but also localizations in endothelial cells. For instance, TAZ is mainly found during the

sprouting front of growing vessels in the nucleus and thus plays an important role in migration. YAP, on the other hand, is more frequently found in the cytoplasm, but not only in sprouting vessels but also in mature vessels, where it influences proliferation (Kim, et al. 2017; Neto, et al. 2018).

Furthermore, our data showed that both calcification media, as well as mechanical stress, induced YAP and TAZ, to respond differently. The influence of mechanical stress was shown by the mRNA data of VEC, in which on one hand, in unstretched cells, CM2 led to a decrease in mRNA expression of YAP and TAZ but on the other hand, in stretched cells, CM2 increased it. In addition, in both, stretched and unstretched VEC, CM1 was observed to cause a change in mRNA expression between YAP and TAZ. CM1 led to an increase in the gene expression of YAP, but at the same time to a decrease in TAZ on mRNA level. Elevated levels of YAP might induce YAP to associate with inhibiting proteins of the TGF-β signaling pathway, such as SMAD7 and SMURF (**fig. 9**), which results in impaired cell growth and differentiation (Piersma, et al. 2015).

Differentiation and activation of osteoblast, and osteogenic lineage progenitor cells is triggered by mechanical stress as part of a physiological process. The proteins Osteoprotegerin (OPG) and Osteopontin (OPN) are, among others, synthesized by cells of the osteogenic lineage (Tanaka, et al. 2003). OPG leads to decreased osteoclast differentiation and activation by binding to RANKL, and thus blocking the RANKL/RANK interaction. This results in higher levels of depositions of hydroxyapatite as they cannot be eliminated by the immune system on its own, and previously formed plaques may increase in size. This whole process can be enhanced by elevated mechanical stress (Tyson, et al. 2020; Udagawa, et al. 2021).

In our data, a significant increase in OPG mRNA expression after treatment with CM1, and even higher gene expression after treatment with CM2, was detected in stretched EC and VEC. In unstretched EC and VEC, the addition of CM1 resulted in a slight increase in mRNA expression of OPG, whereas after treatment with CM2, there was a slight increase in EC and a decrease in VEC in the expression of OPG on mRNA level. Considering, there was a significant increase in mRNA expression of OPG in stretched cells, but only a slight increase or decrease in unstretched cells, our data confirm the hypothesis of Tyson, *et al.*, describing that mechanical stress accelerates the process described above (Tyson, et al. 2020; Udagawa, et al. 2021).

OPN is an extracellular matrix cell adhesion protein that has been identified to be expressed in response to mechanical stress (Okamoto 2007). Furthermore, OPN is associated with inflammatory diseases and serves as a marker for mineralization (Quaglino, et al. 2020). Canfield, Farrington *et al.* referred OPN as an anticalcification factor, as their studies showed that mineralization of heart valves is opposed by Osteopontin, binding to apatite (Canfield, et al. 2002). My data support these insights, showing that cyclic stretch and treatment with CM1 increased mRNA expression of OPN in EC. In VEC, similar effects were observed, even in unstretched cells.

Analysis of protein expression of OPG and OPN by Western blots showed no specific bands. This may be due to the fact that our primary-antibodies were not able to bind to the proteins OPG and OPN, as they are directed against epitopes of human antigens. Another possibility is that the proteins OPG and OPN have not been synthesized in the cells yet. To determine the cause of the absent bands, further Western blots with specific antibodies directed against porcine epitopes need to be performed.

6. Summaries

6.1. English

Vascular and valvular calcification often represents a pathological background of vascular diseases and thus can lead to serious health problems. Vascular calcification is an actively controlled multifactorial process and is characterized as mineral deposition in the form of calcium and phosphate complexes.

This work aimed to explore the relationship between primary porcine endothelial cells, calcification, and mechanical stress through the resultant expression of *YAP, TAZ, OPN,* and *OPG. YAP* and *TAZ* are effectors of the Hippo pathway, that is related to cell proliferation, tissue growth, wound healing, regeneration, and cell survival under stress, while *OPG* and *OPN* are more directly related to calcification and mainly expressed by cells of the osteogenic lineage.

For my project, porcine vascular and valvular endothelial cells (EC and VEC) were treated with organic and inorganic calcification media to induce calcification *in vitro*. In order to mimic mechanical stress, cells - cultured with and without calcification media – were subjected to cyclic stretch by a FlexCell FX-5000^{TM} device. Afterward, we compared the expression of calcification related genes of these cells, using molecular biological assays, like qPCR and Western blots. In addition, immunohistochemical staining was performed to further characterize the cells.

My results show a clear correlation between increased mechanical stress and calcification. Furthermore, it could be observed that not only endothelial cells of the aorta and endothelial cells of cardiac valves respond differently to mechanical stress, there is also a difference whether organic or inorganic phosphate was used to induce calcification.

With this work, I want to contribute to a better understanding of the different mechanisms and influences involved in the multifaceted process of calcification in order to help discover new therapeutic approaches to treat or reverse vascular and valvular calcification in a more targeted way in the future.

6.2. Deutsch

Gefäß- und Klappenverkalkungen stellen häufig einen pathologischen Hintergrund von Gefäßerkrankungen dar und können somit zu schwerwiegenden gesundheitlichen Problemen führen. Vaskuläre Verkalkung ist ein aktiv gesteuerter multifaktorieller Prozess und ist als Mineralablagerung in Form von Kalzium- und Phosphatkomplexen gekennzeichnet.

Ziel dieser Arbeit war es, die Beziehung zwischen primären porcinen Endothelzellen, Verkalkung und mechanischem Stress anhand der resultierenden Expression von *YAP*, *TAZ*, *OPG* und *OPN* zu analysieren. *YAP* und *TAZ* sind Effektoren des Hippo-Signalweges, der mit Zellproliferation, Gewebewachstum, Wundheilung, Regeneration und Überleben der Zellen unter Stress in Verbindung steht, während *OPG* und *OPN* vor allem von Zellen der osteogenen Linie exprimiert werden und in direkterem Zusammenhang mit Verkalkung stehen.

Für mein Projekt wurden porcine vaskuläre und valvuläre Endothelzellen (EC und VEC) mit organischen und anorganischen Kalzifizierungsmedien behandelt, um Kalzifizierung *in vitro* zu induzieren. Um mechanischen Stress zu imitieren, wurden die Zellen, die jeweils mit und ohne Kalzifizierungsmedium kultiviert wurden, einer zyklischen Dehnung mit einem FlexCell FX-5000TM Gerät ausgesetzt. Anschließend verglichen wir die Expression der Gene *YAP*, *TAZ*, *OPG* und *OPN* dieser Zellen mit Hilfe molekularbiologischer Assays wie qPCR und Western Blots. Darüber hinaus wurde eine immunhistochemische Färbung durchgeführt, um die Zellen zu charakterisieren.

Meine Ergebnisse zeigen eine Korrelation zwischen erhöhter mechanischer Belastung und Verkalkung. Darüber hinaus konnte beobachtet werden, dass nicht nur Endothelzellen der Aorta und Endothelzellen der Herzklappen unterschiedlich auf mechanischen Stress reagieren, sondern auch dass es auch einen Unterschied macht, ob organisches oder anorganisches Phosphat verwendet wurde, um Verkalkung zu induzieren.

Mit dieser Arbeit möchte ich zu einem besseren Verständnis der verschiedenen Mechanismen und Einflüsse beitragen, die an dem vielseitigen Prozess der Verkalkung beteiligt sind, damit in Zukunft weitere therapeutische Ansätze entwickelt werden können, mit denen sich Gefäß- und Herzklappenverkalkungen gezielter behandeln oder rückgängig machen lassen.

7. References

Allison, M. A., M. H. Criqui, and C. M. Wright

2004 Patterns and risk factors for systemic calcified atherosclerosis. Arterioscler Thromb Vasc Biol 24(2):331-6.

Boyce, B. F., and L. Xing

2008 Functions of RANKL/RANK/OPG in bone modeling and remodeling. Arch Biochem Biophys 473(2):139-46.

Canfield, A. E., et al.

2002 The involvement of matrix glycoproteins in vascular calcification and fibrosis: an immunohistochemical study. J Pathol 196(2):228-34.

Falk, E.

2006 Pathogenesis of atherosclerosis. J Am Coll Cardiol 47(8 Suppl):C7-12.

Fatherazi, S., et al.

2009 Phosphate regulates osteopontin gene transcription. J Dent Res 88(1):39-44.

Gregory, C. A., et al.

2004 An Alizarin red-based assay of mineralization by adherent cells in culture: comparison with cetylpyridinium chloride extraction. Anal Biochem 329(1):77-84.

Hu, H. H., et al.

2018 New insights into TGF-β/Smad signaling in tissue fibrosis. Chem Biol Interact 292:76-83.

Hutcheson, J. D., E. Aikawa, and W. D. Merryman

2014 Potential drug targets for calcific aortic valve disease. Nat Rev Cardiol 11(4):218-31.

Icer, M. A., and M. Gezmen-Karadag

2018 The multiple functions and mechanisms of osteopontin. Clin Biochem 59:17-24.

Johnson, R. C., J. A. Leopold, and J. Loscalzo

2006 Vascular calcification: pathobiological mechanisms and clinical implications. Circ Res 99(10):1044-59.

Kawakami, R., et al.

2016 RANKL system in vascular and valve calcification with aging. Inflamm Regen 36:10.

Kim, J., et al.

2017 YAP/TAZ regulates sprouting angiogenesis and vascular barrier maturation. J Clin Invest 127(9):3441-3461.

Ma, S., et al.

2019 The Hippo Pathway: Biology and Pathophysiology. Annu Rev Biochem 88:577-604.

Mathieu, P., R. Bouchareb, and M. C. Boulanger

2015 Innate and Adaptive Immunity in Calcific Aortic Valve Disease. J Immunol Res. 2015:851945.

Meng, Z., T. Moroishi, and K. L. Guan

2016 Mechanisms of Hippo pathway regulation. Genes Dev 30(1):1-17.

Neto, F., A. Klaus-Bergmann, and Y. T. Ong

2018 YAP and TAZ regulate adherens junction dynamics and endothelial cell distribution during vascular development. Elife7, 2018;7:e31037.

Okamoto, H.

2007 Osteopontin and cardiovascular system. Mol Cell Biochem 300(1-2):1-7.

Piccolo, S., S. Dupont, and M. Cordenonsi

2014 The biology of YAP/TAZ: hippo signaling and beyond. Physiol Rev 94(4):1287-312.

Piersma, B., R. A. Bank, and M. Boersema

2015 Signaling in Fibrosis: TGF-β, WNT, and YAP/TAZ Converge. Front Med (Lausanne) 2:59.

Pocaterra, A., and P. Romani

2020 YAP/TAZ functions and their regulation at a glance. J Cell Sci 133(2).

Pugsley, M. K., and R. Tabrizchi

2000 The vascular system. An overview of structure and function. J Pharmacol Toxicol Methods 44(2):333-40.

Quaglino, D., F. Boraldi, and F. D. Lofaro

2020 The biology of vascular calcification. Int Rev Cell Mol Biol 354:261-353.

Rutkovskiy, A., et al.

2019 Mechanical stress alters the expression of calcification-related genes in vascular interstitial and endothelial cells. Interact Cardiovasc Thorac Surg 28(5):803-811.

Rutkovskiy, A., et al.

2017 Valve Interstitial Cells: The Key to Understanding the Pathophysiology of Heart Valve Calcification. J Am Heart Assoc 6(9).

Spicer, D. E., et al.

2014 The anatomy and development of the cardiac valves. Cardiol Young 24(6):1008-22.

Tanaka, S. M., et al.

2003 Effects of broad frequency vibration on cultured osteoblasts. J Biomech 36(1):73-80.

Totaro, A., T. Panciera, and S. Piccolo

2018 YAP/TAZ upstream signals and downstream responses. Nat Cell Biol 20(8):888-899.

Tyson, J., et al.

2020 Mechanisms of the Osteogenic Switch of Smooth Muscle Cells in Vascular Calcification: WNT Signaling, BMPs, Mechanotransduction, and EndMT. Bioengineering (Basel) 7(3).

Udagawa, N., et al.

2021 Osteoclast differentiation by RANKL and OPG signaling pathways. J Bone Miner Metab 39(1):19-26.

Venuraju, S. M., et al.

2010 Osteoprotegerin as a predictor of coronary artery disease and cardiovascular mortality and morbidity. J Am Coll Cardiol 55(19):2049-61.

Yu, F. X., B. Zhao, and K. L. Guan

2015 Hippo Pathway in Organ Size Control, Tissue Homeostasis, and Cancer. Cell 163(4):811-28.

Yuan, C., et al.

2021 Vascular calcification: New insights into endothelial cells. Microvasc Res 134:104105.

Zhang, Y., and X. Wang

2020 Targeting the Wnt/β-catenin signaling pathway in cancer. J Hematol Oncol 13(1):165.

Zheng, Y., and D. Pan

2019 The Hippo Signaling Pathway in Development and Disease. Dev Cell 50(3):264-282.

8. Appendix

8.1. List of figures

8.2. List of tables

8.3. List of abbreviation

Abbreviation	Full term
APC	Adenomatous polyposis coli
APS	Ammonium persulfate
BMP	Bone morphogenetic protein
BSA	Bovine serum albumin
CD31	platelet endothelial cell adhesion molecule-1
CK1	casein kinase 1
CM1/2	Calcification medium1/2
CO	Control
CT	Cycle threshold
DAPI	4′,6-diamidino-2-phenylindole
DC	Duty cycle
DDT	Dichlorodiphenyltrichloroethane
DEPC	Diethyl pyrocarbonate
DMEM	Dulbecco's Modified Eagle Medium
DMSO	Dimethyl sulfoxide
DVL	Disheveled
EC	Vascular endothelial cells
ECGS	Endothelial Cell Growth Supplement
ECL	Enhanced chemiluminescence
ECM	Extracellular matrix
EDTA	Ethylene diamine tetraacetic acid
EMT	Epithelial-to-mesenchymal transition
FBS	Fetal bovine serum
Freq	Frequency
GSK3	Glycogen synthase kinase 3
HRP	Horseradish peroxidase HRP
LATS1/2	Large tumor suppressor
LEF	Lymphoid enhancer factor
LRP5/6	Lipoprotein-related-receptor protein
MOB1A/B	MOB kinase activator 1A/B
MST1/2	Mammalian Ste20-like kinase1/2
OD	Optical density
OPG	Osteoprotegerin
OPN	Osteopontin

PBS	Phosphate-buffered saline
Pen/Strep	Penicillin-Streptomycin
PVDF	polyvinylidene difluoride
RANK	Receptor activator of nuclear factor κ B
RANKL	Receptor activator of nuclear factor kappa-B ligand
rpm	Rounds per minute
RT	Room temperature
SAV1	Salvador family WW domain-containing protein 1
SD	Standard deviation
SDS	Sodium dodecyl sulfate
Smurf	Smad-specific E3 ubiquitin-protein ligases
TAZ	Transcriptional coactivator with PDZ-binding motif
TBS	Tris-buffered saline
TCF	T cell factor
TEAD1—4	TEA domain transcription factors 1—4
TEMED	N,N,N',N'-tetramethylenediamine
TGF-β	Transforming growth factor-β
VEC	Valvular endothelial cells
VWF	Von Willebrand factor
Wnt pathway	Wingless/Ints pathway
YAP	Yes-associated protein
α-SMA	α-smooth muscle actin
β-TrCP	Beta-transducin repeat containing E3 ubiquitin protein ligase